SAND REPORT

SAND2003-0094
Unlimited Release
Printed January 2003

Radiation-Induced Prompt Photocurrents in Microelectronics: Physics

Paul E. Dodd, Gyorgy Vizkelethy, Wendland Beezhold, David S. Walsh, Daniel L. Buller, and Barney Doyle

Prepared by
Sandia National Laboratories
Albuquerque, New Mexico 87185 and Livermore, California 94550

Sandia is a multiprogram laboratory operated by Sandia Corporation,
a Lockheed Martin Company, for the United States Department of Energy's
National Nuclear Security Administration under Contract DE-AC04-94-AL85000.

Issued by Sandia National Laboratories, operated for the United States Department of Energy by Sandia Corporation.

Available to DOE and DOE contractors from
U.S. Department of Energy
Office of Scientific and Technical Information
P.O. Box 62
Oak Ridge, TN 37831

Telephone: (865)576-8401
Facsimile: (865)576-5728
E-Mail: reports@adonis.osti.gov
Online ordering: http://www.doe.gov/bridge

Available to the public from
U.S. Department of Commerce
National Technical Information Service
5285 Port Royal Rd
Springfield, VA 22161

Telephone: (800)553-6847
Facsimile: (703)605-6900
E-Mail: orders@ntis.fedworld.gov
Online order: http://www.ntis.gov/help/ordermethods.asp?loc=7-4-0#online

SAND2003-0094
Unlimited Release
Printed January 2003

Radiation-Induced Prompt Photocurrents in Microelectronics: Physics

Paul E. Dodd
Radiation Physics, Simulation, and Technology

Gyorgy Vizkelethy, David S. Walsh, Daniel L. Buller, and Barney Doyle
Radiation Solid Interactions and Processing Department

Sandia National Laboratories
P.O. Box 5800
Albuquerque, NM 87185-1083

Wendland Beezhold
Idaho State University
Department of Physics
Pocatello, ID 83209

Abstract

The effects of photocurrents in nuclear weapons induced by proximal nuclear detonations are well known and remain a serious hostile environment threat for the US stockpile. This report describes the final results of an LDRD study of the physical phenomena underlying prompt photocurrents in microelectronic devices and circuits. The goals of this project were to obtain an improved understanding of these phenomena, and to incorporate improved models of photocurrent effects into simulation codes to assist designers in meeting hostile radiation requirements with minimum build and test cycles. We have also developed a new capability on the ion microbeam accelerator in Sandia's Ion Beam Materials Research Laboratory (the Transient Radiation Microscope, or TRM) to supply ionizing radiation in selected micro-regions of a device. The dose rates achieved in this new facility approach those possible with conventional large-scale dose-rate sources at Sandia such as HERMES III and Saturn. It is now possible to test the physics and models in device physics simulators such as Davinci in ways not previously possible. We found that the physical models in Davinci are well suited to calculating prompt photocurrents in microelectronic devices, and that the TRM can reproduce results from conventional large-scale dose-rate sources in devices where the charge-collection depth is less than the range of the ions used in the TRM.

Contents

Figures

Tables

This page intentionally left blank.

Introduction

The effects of photocurrents in nuclear weapons induced by proximal nuclear detonations are well known and remain a serious hostile environment threat for the US stockpile. The focus of this LDRD was to study the physical phenomena underlying prompt photocurrents in microelectronic devices and circuits. The goal of this LDRD was to obtain an improved understanding of these phenomena, and to incorporate improved models of photocurrent effects into simulation codes to assist designers in meeting hostile radiation requirements with minimum build and test cycles. Empirical studies require variations in processing and design that are both expensive and time consuming. Validated model-based design trade-off studies can be significantly cheaper, with months to years shorter development times. Better radiation-hardened devices can be made by clearly understanding the physics of their response and the trade-offs between photocurrent sensitivity, performance, and process complexity.

Over the past three years, three important developments have occurred which, when combined, now provide Sandia with a powerful new way to study, predict, and design devices and circuits which control and minimize prompt photocurrent effects.

The first has been the continuing development and application of various Radiation Microscopies (RMs) on Sandia's Tandem-accelerator microbeam [1]. Prior to this work, these RM techniques involved the controlled exposure of electronic components to highly focused individual heavy ions. Single-event upset (SEU) imaging has been extensively used to address the reliability concerns for space-based and weapon electronics due to naturally occurring energetic heavy ions in the space environment. Data obtained using the focused ion microbeam have enabled the diagnoses of microcircuit vulnerabilities to SEU that are simply unobtainable using standard broadbeam techniques. For example, by scanning a focused ion beam across an operating IC, we can detect the actual physical locations on the IC that are sensitive to SEU. This technique has been invaluable for diagnosing unexpected SEU failure modes in Sandia-fabricated devices. By pinpointing sensitive locations, SEU imaging has resulted in significant cost savings for redesigning radiation-hardened ICs and has enabled the achievement of improved SEU hardness levels.

The second development is the improvement of physics-based 3D device simulation tools. Analytical photocurrent models have been successfully applied for low-level transients. At higher radiation dose rates, effects such as the variation of lifetime and carrier mobility with injection level, internal electric field distortions, and Auger recombination become important. These effects are typically ignored in analytical models. Numerical device simulators work at a fundamental physical level and inherently handle phenomena such as electric field distortions and high injection conditions. Until recently, device models could study the effects of radiation only on single, isolated devices or test structures. With mixed-level device and circuit simulators, the response of entire circuit fragments can be simulated. Using the enhanced capability of ASCI-level calculations, much larger portions of a circuit can be simulated in the multidimensional device domain, an important improvement for dose-rate situations where radiation-induced carriers flood the entire device or integrated circuit. A promising numerical device and circuit level simulator for high dose-rate, prompt photocurrent conditions is Davinci [2,3]. Davinci is a commercial 3D numerical simulator used by semiconduc-

tor chip manufacturers to optimize transistor fabrication techniques and designs. However, Davinci, used at Sandia primarily for cosmic-ray upset analysis, had not been rigorously applied to (nor validated for) the study of x-ray and gamma-ray photocurrents. The accuracy of these models was therefore unknown for charge transport in high-radiation dose-rate environments. Possible deficiencies included the variation of lifetime with carrier injection level, internal electric fields, and the variation of mobility and diffusion constants with injection level.

The third development, and the subject of this LDRD, is using Sandia's Tandem microbeam to generate single pulses of ions to simulate dose-rate transients in weapons environments. Conventional dose-rate testing utilizes large-scale irradiation facilities such as electron beam linear accelerators (LINACs) or large flash x-ray sources to irradiate individual discrete devices or integrated circuits (ICs). Indeed, many of these facilities were designed to irradiate entire assemblies or subassemblies. Unfortunately, three-dimensional physics-based simulation tools can calculate the photocurrent response of a single microelectronic device, or at most a few transistors. This gap between the experimental dose-rate response at the IC level and the calculated response at the individual transistor level presents a challenge for directly validating device simulators with experimental data.

Under this LDRD, we have developed a new capability on the ion microbeam accelerator in Sandia's Ion Beam Materials Research Laboratory (the Transient Radiation Microscope, or TRM) to supply ionizing radiation in selected micro-regions of a device. We have demonstrated dose rates approaching those possible with conventional large-scale simulators at Sandia such as Sphinx, HERMES III, and Saturn. It is therefore possible to test the physics and models in Davinci at the device or subcircuit level in ways not previously possible. This new capability, which we call Transient Radiation Microscopy (TRM), makes possible for the first time the direct validation of 3D numerical models for the prediction of prompt photocurrents at the device level.

Using Ion Beams to Simulate Photocurrent Response

The Ion Microbeam at Sandia New Mexico

The ion microbeam is located in the Ion Beams Materials Research Lab (IBMRL) at Sandia National Laboratories, New Mexico. The IBMRL was developed primarily as a facility for material analysis and the ion microbeam makes it a unique facility for both IBA and radiation effects microscopy. Figure 1 shows a schematic layout of the IBMRL with the four ion sources, the 6 MV EN tandem Van de Graaff accelerator and analyzing magnet for the eight beam lines. Many techniques are available at the IBMRL:

Ion Beam Analysis (IBA)

- Rutherford Backscattering Spectrometry (RBS)
- Proton Induced X-ray Emission (PIXE)
- Nuclear Reaction Analysis (NRA)
- Elastic Recoil Detection (ERD)

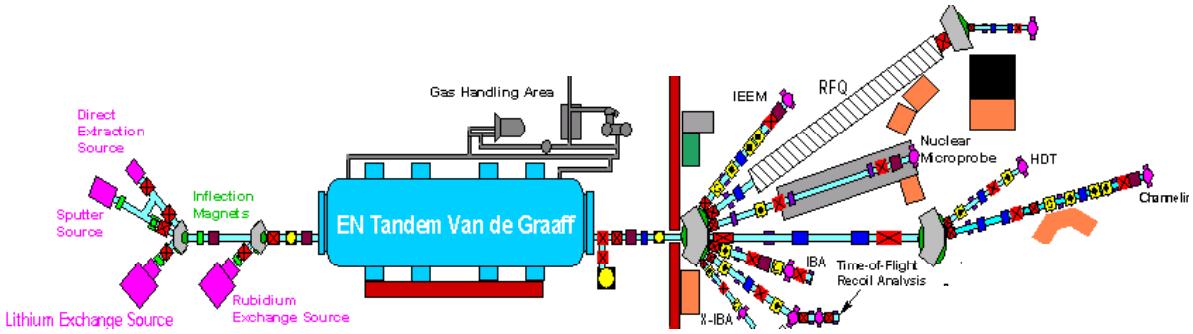

Figure 1. Schematic layout of the IBMRL at Sandia, New Mexico. A number of ion beam analysis techniques and radiation effects studies can be performed on various beam lines.

- Heavy Ion Backscattering Spectrometry (HIBS)

Radiation Effects Microscopy (REM)

- Single Event Upset Imaging (SEU-Imaging)
- Ion Beam Induced Charge Collection (IBICC)
- Time Resolved IBICC (TRIBICC)
- Ion Electron Emission Microscopy (IEEM)

Other lab capabilities

- RFQ Booster of 1.9 MeV/amu for use in high-LET SEU testing
- External Ion Beam Analysis for large and non-vacuum-compatible samples

Proof of Concept: The Mark I Transient Radiation Microscope (TRM)

The original TRM system was comprised of five major elements, as illustrated in Figure 2 [4]:

1) The 6 MV EN tandem Van de Graaff accelerator to provide the beam of high-energy heavy ions
2) A beam pulsing system to time-focus these ions
3) The beam defining slits and magnetic quadrupole double lens for focusing the ions
4) A target chamber and manipulator system that will handle the device under test (DUT) and provide feedthroughs for the electronic signals
5) The measurement and data acquisition system to capture and analyze current transients resulting from the pulse of heavy ions that strike the sample

The 6 MV EN tandem Van de Graaff accelerator provides an input beam of high-energy heavy ions. The beam is normally deflected off the device under test (DUT) and blocked by some defining slits. Upon demand, the data collection system provides a control pulse to a high voltage pulser which quickly changes the bias on the deflection plates in the beamline and sweeps the beam onto the DUT. The minimum beam pulse-width is limited by the high

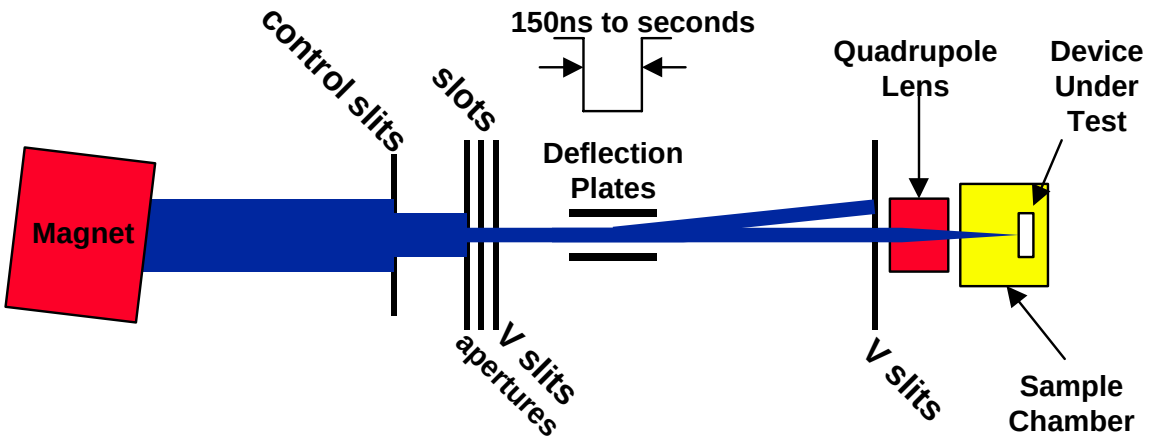

Figure 2. Schematic of the Mk. I Transient Radiation Microscope (TRM). The microbeam line length is ~9 m as measured from the switching magnet. 6 kV deflector plates move the ion beam into and back out of the object slits to produce a transient radiation pulse. The Tandem accelerator, not shown, is to the left of the magnet.

voltage pulser response time to ~150 ns duration. The pulse of ions is magnetically focused to a spot diameter between 50-500 μm by a quadrupole double lens. The induced current transients in the device are measured using fast (1 or 4.5 GHz) digitizing scopes and stored by the data acquisition computer. The target manipulator system is capable of ±5 μm position resolution and has continuous optical microscopic viewing, which enables the experimenter to dose specific regions on the DUT.

The First TRM Experiments

We performed the first-ever transient radiation microscopy experiments using a commercially-available Hamamatsu S1223 PIN diode. The Hamamatsu PIN diode has a large area (3.6 mm×3.6 mm) and a deep intrinsic region (316.5 μm). We selected this PIN diode first because these PINs had been previously used as tuning diodes for single-event upset work and thus were readily available. The test fixture used for the experiments conformed to the ASTM Standard (F675-91) for measuring transient photocurrents in p-n junctions. The ion beam had a pulsewidth of 200-250 ns, with a rise time of 20 ns and a fall time of 25 ns. Photocurrent transients were recorded across 50 Ω on a Tektronix 680B digital oscilloscope and saved with an in-house data acquisition system. A 5-V 200-ns pulse triggered the beam deflector and the digital oscilloscope.

The initial TRM data runs were conducted using 35-MeV Cl ions. This ion species and energy were chosen for several reasons. First, Cl is one of the most abundant beams available from the tandem accelerator, which is necessary to achieve high dose rates. Second, it can be reasonably easily focused with the microbeam quadrupole lens. Third, 35-MeV Cl ions have a range of ~10 μm in Si, which was initially believed to deposit all charge in the device regions of interest.

Figures 3 and 4 show some of the first TRM data taken of the photocurrent response of a commercial Hamamatsu S1223 PIN diode with an active area of 3.6 mm x 3.6 mm. Surprisingly, in most cases the measured photocurrent response was much longer than the duration of the radiation pulse itself. For example, in Figure 3 only the 25-V bias photocurrent response follows the deflector pulse, while both responses shown in Figure 4 are much longer than the incident heavy ion pulse. Figure 4 is for a high dose rate of 1.2×10^{11} rad(Si)/s while Figure 3 is for a much lower dose rate of 4.7×10^{7} rad(Si)/s. The extremely long storage times observed were an unexpected result, and had not been seen in previous testing at SPHINX.

The dose rate that can be achieved using the system depends on the ion being accelerated (heavier ions produce higher dose rates), the particle beam current, and the beam diameter. The dose rate capability of the Mk I TRM system for five different ion species is displayed in Figure 5 for beam diameters of 60 µm. As mentioned, the maximum dose rate achievable increases for heavier ions such as chlorine. In general, the higher the linear energy transfer (LET) of the particle, the higher the achievable dose rate. Another important factor is how abundant the beam is in the accelerator (i.e., the maximum beam particle current that can be obtained). With especially abundant beams, higher dose rates can be achieved by increased beam current, in spite of lower particle LET (e.g., Si ions in Figure 5). However, as dose rate increases, the particle range in the target material (in this case silicon) in general decreases. For example, as shown in Figure 5, chlorine ions have a range in silicon of only ~10 µm. This has implications on the photocurrent response of devices that can collect charge generated deep within the device, as will be discussed later. Ions accelerated in the Mk I system included protons, helium, carbon, silicon, and chlorine, and dose rates on the order of one to a few hundred Grad(Si)/s were demonstrated.

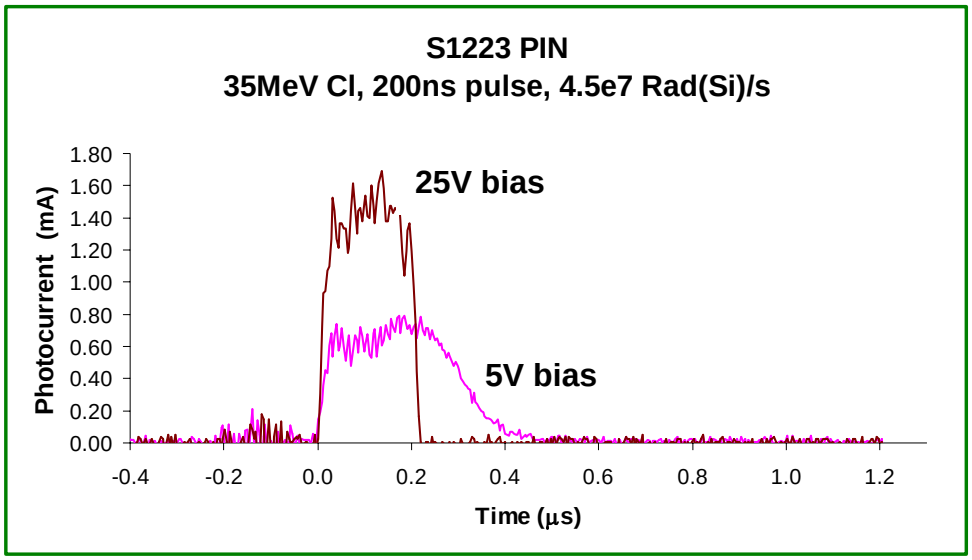

Figure 3: TRM photocurrent response of a Hamumatsu S1223 PIN photodiode. Photocurrent (in mA) is shown as a function of reverse bias for a beam diameter of 500 µm using 35-MeV Cl ions in a single pulse of 200 ns width. The calculated dose rate is 4×10^{7} rad(Si)/s.

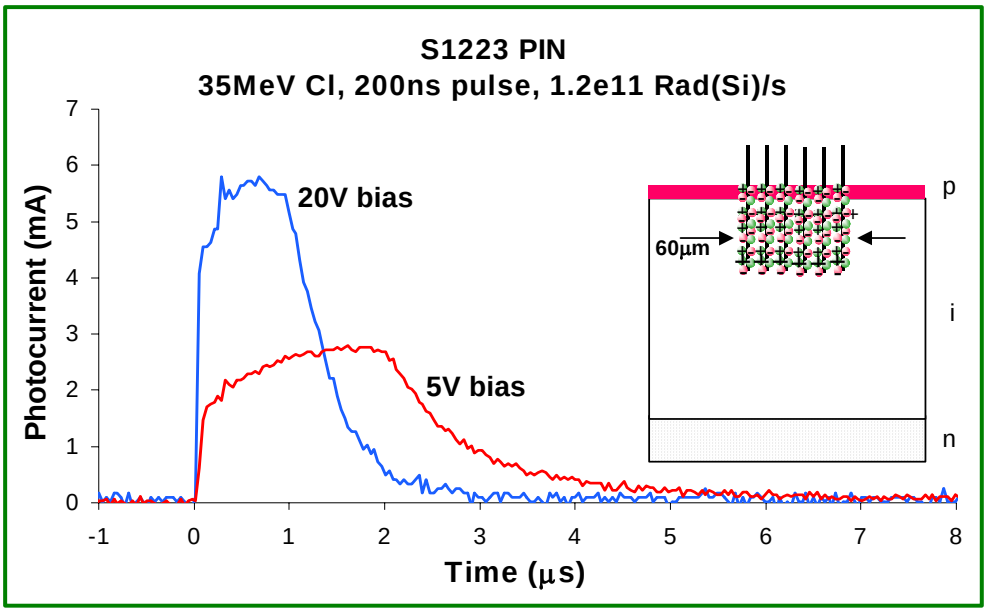

Figure 4. TRM photocurrent response of a Hamumatsu S1223 PIN photodiode at high dose rate. The photocurrent (in mA) is shown as a function of reverse bias for a beam diameter of 60 µm using 35-MeV Cl ions in a single pulse of 200 ns width. The calculated dose rate is 1.2×10^{11} rad(Si)/s.

Figure 6 illustrates our original projections of how the TRM microbeam capability complements other radiation sources for photocurrent generation. Saturn, for example, is a facility of choice for large test areas and subsystem testing. Sphinx is very desirable for testing at the device level. The microbeam is best suited for only small regions of a device or very small devices. In Mark-I configuration, the TRM is capable of dose rates on the order of a few tenths of a Trad(Si)/s (100 Grad(Si)/s) with pulse widths of 200 ns. As shown in Figure 6, this compares very favorably with the SPHINX and SATURN facilities, but the TRM system allows precisely targeted small-area irradiation of single devices. The TRM therefore complements almost perfectly the capabilities of SPHINX and SATURN.

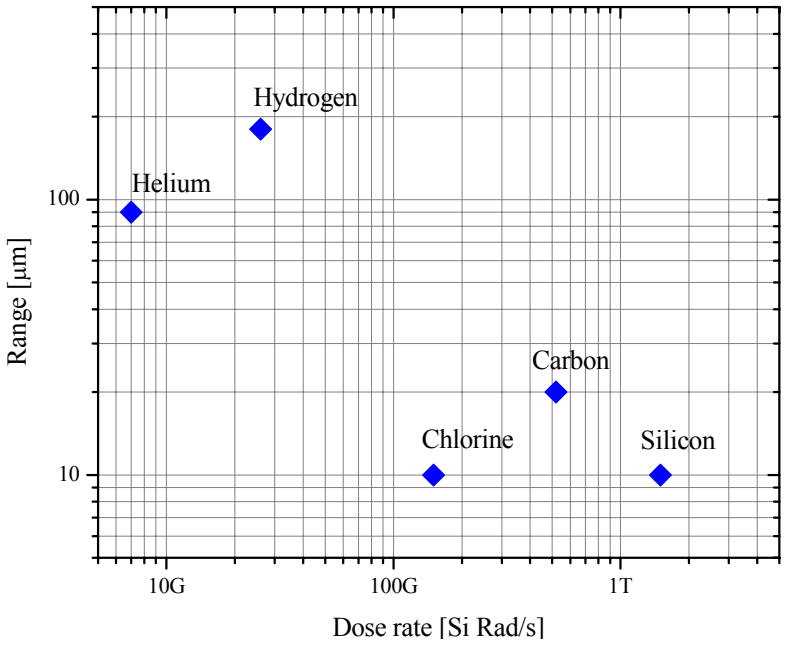

Figure 5. Tradeoff between dose rate and maximum ion penetration depth (range in µm) into Si available in the TRM.

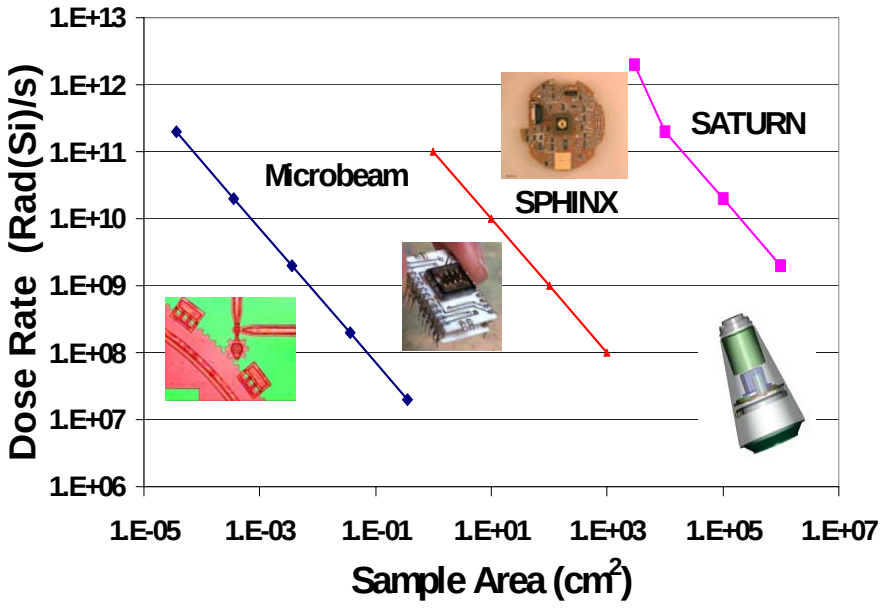

Figure 6. Dose rate versus sample area for transient dose-rate test facilities.

TRM Issues

We now discuss a number of issues we identified in the Mk I TRM regarding using the ion microbeam as a dose-rate radiation effects simulator for photocurrent testing. A partial list includes the following:

Noise: As may be observed in Figure 3, the noise level is on the order of ±0.2 mA for the 1.40 mA photocurrent at 25 V bias. Without reducing this noise, which seems to be ringing from the beam-switching HV power supply, the Mk I TRM was limited to measuring photocurrents above ~0.3 mA. Figure 7 illustrates these limits by the vertical error bars at low dose rates.

Ion beam current error: A more serious problem at low dose rates is our present lack of accuracy in measuring ion beam currents below 2 nA. At present, we calculate dose rate directly from knowledge of the ion beam energy, E, and the ion current, I_b. For the chlorine beam, the ion energy, E, is 35±0.01 MeV, however our error in measuring I_b is ±1 nA. The horizontal error bars in Figure 7 illustrate this point. Below about $2x10^7$ rad(Si)/s dose rate, we could not accurately calculate the equivalent dose rate because of the error in measuring ion beam current.

Permanent ion damage: Unlike traditional dose-rate sources, the ion microbeam causes significant displacement damage in the semiconductor crystal lattice. Because of this, the total exposure dose in the TRM must be carefully monitored. Figure 8 plots the predicted limit of dose before the onset of device damage. This calculated limit assumes a maximum of 10^7 displacements per atom in an IC can be tolerated before damage-induced vacancies cause device performance deviations [4]. Note that this very ion damage might be used to simulate neutron damage effects and recent work shows that variable pulse length TRM might indeed be useful in such a mode.

Ion ionizing dose equivalent to gamma dose: Figure 9 illustrates the qualitative difference between gamma-ray irradiation and ion-beam bombardment. Each gamma or x-ray yields a diffuse energy deposition through scattering and electron-photon transport. In contrast, each ion produces a narrow column of electron-hole pairs, however the net effect of many ions may give the same final result as far as collected charge, or photocurrent, is concerned.

Dose rate and pulse length limits: The upper limit to achievable dose rate is only limited by maximum beam currents. Table 1 lists the most prolific ion beams available in the San-

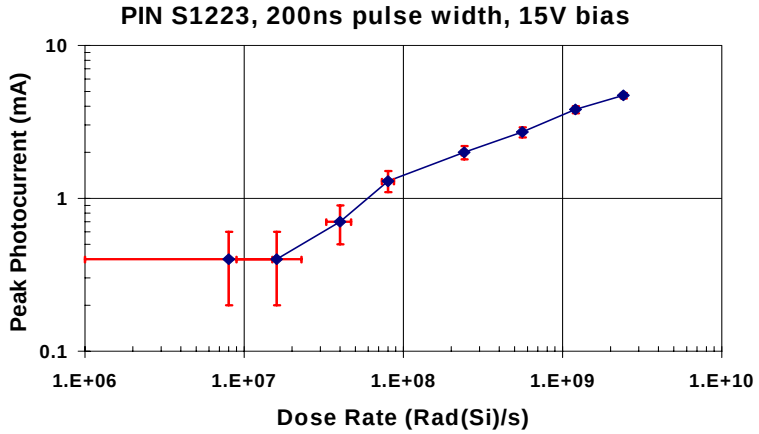

Figure 7. Low dose rate measurements are limited by errors in beam current (horizontal error bars) and noise (vertical error bars) in the measured photocurrent response.

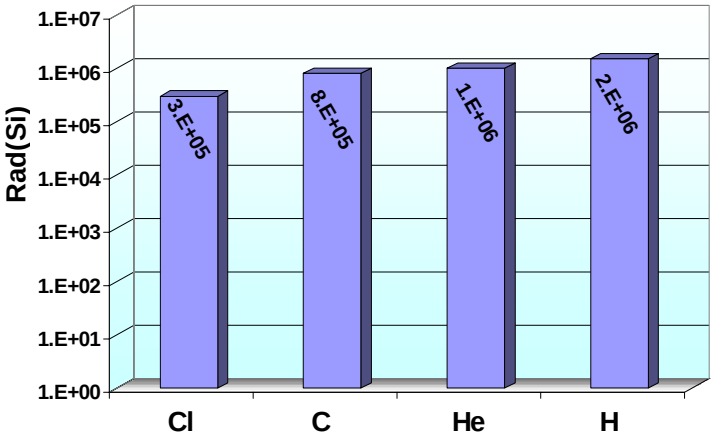

Figure 8. Total dose limit in Si before damage of device for beams available. This calculation assumes that a maximum of 10^7 displacements per atoms can be tolerated before device degradation.

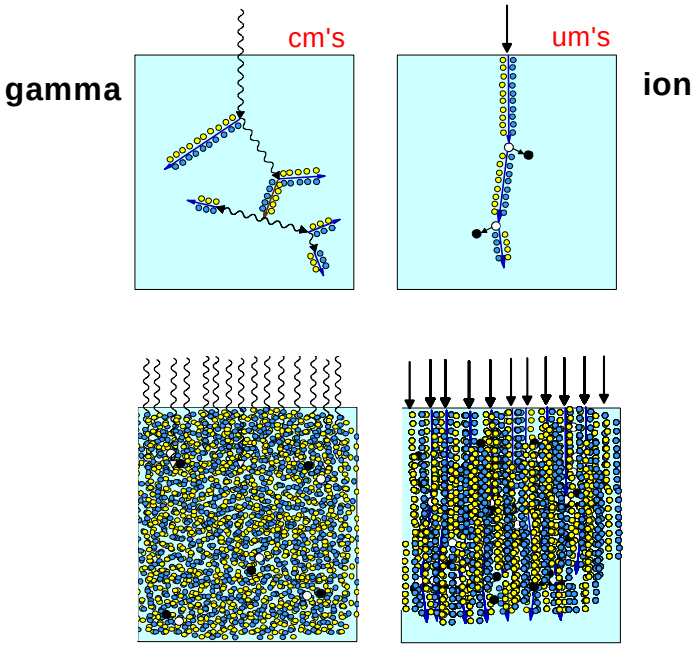

Figure 9. The physics and scale of charge generation caused by gamma rays vs. ions is different, but the net effect is expected to be similar.

dia microbeam. An advantage of the TRM system is that any pulse width longer than 150 ns (up to DC) is very easily reachable by simply leaving the beam on the DUT for the desired time. On the other hand, the short pulse length in the Mk I TRM was limited by the 150-ns HV switching power supply. Alternative configurations to reduce the pulse width considered early on included a 50-ns pulse length power supply or a beam buncher to attain sub-20-ps pulse widths.

Table 1: Most abundant ion beams available at the Sandia microbeam.

Ion Beam	Energy (MeV)	Est. Max Current (particle nA)	Range in Si (μm)	Est. Max Dose Rate (rads/s)
H	4.5	100	180	3×10^{10}
He	12	10	90	7×10^{9}
C	20	30	20	5×10^{11}
Cl	35	2	10	1.5×10^{11}
Si	28	25	10	1.5×10^{12}

Development of a Routine TRM Capability

Production Testing: The Mark II TRM

Having successfully developed and demonstrated the concept for a transient radiation microscope, the next step involved developing a robust and usable TRM for more "production-like" testing. Equally important was exercising the system, understanding how the results would compare to broad beam dose-rate sources, and comparing TRM results to Davinci calculations. While the Mark I TRM was a "proof of principle" system, the Mark II TRM was developed to be a production system. A new beam chamber (described below) enables us to position the device under test (DUT) quickly, reproducibly and with high precision in the x and y direction (<100 nm). Several samples can be mounted in the chamber at the same time, which makes the experiments much faster than in the Mk I TRM. A Faraday cup was mounted close to the upstream side of the focusing magnet to measure the current before each shot. This was calibrated using a high precision Faraday cup on the target holder. This way the precision of the current measurement (which was a serious problem in the Mk I TRM, as previously described) has been greatly improved, up to 5-10%. Another significant problem in the Mk I TRM was a high noise level, which prohibited low dose rate measurements. Most of this noise has been eliminated in the Mk II TRM. In order to improve the strength of our deflection system we placed the deflection plates only 0.2" apart, which allowed us to use lower deflection voltages and further reduce the noise level.

The minimum gate pulse that can be input using the Mark II TRM is 100 ns, but this results in somewhat larger than 100 ns actual beam pulses. This is illustrated in Fig. 10, which shows the input signal to the high-voltage pulser, as well as the Hamamatsu PIN diode response for an exposure at a dose rate of 2.4×10^{9} rad(Si)/s. The beam used consisted of 35-MeV Cl^{+6} ions. Both curves have been normalized so they can by plotted on the same graph. At this low dose rate, the PIN diode response is expected to directly mirror the beam pulse, and the steep trailing edge of the diode response is an indication that it does so. This data therefore suggests that although the input pulse is about 150 ns in duration, the actual beam pulsewidth for this exposure is closer to 250 ns. The fact that the pulse width has spread to

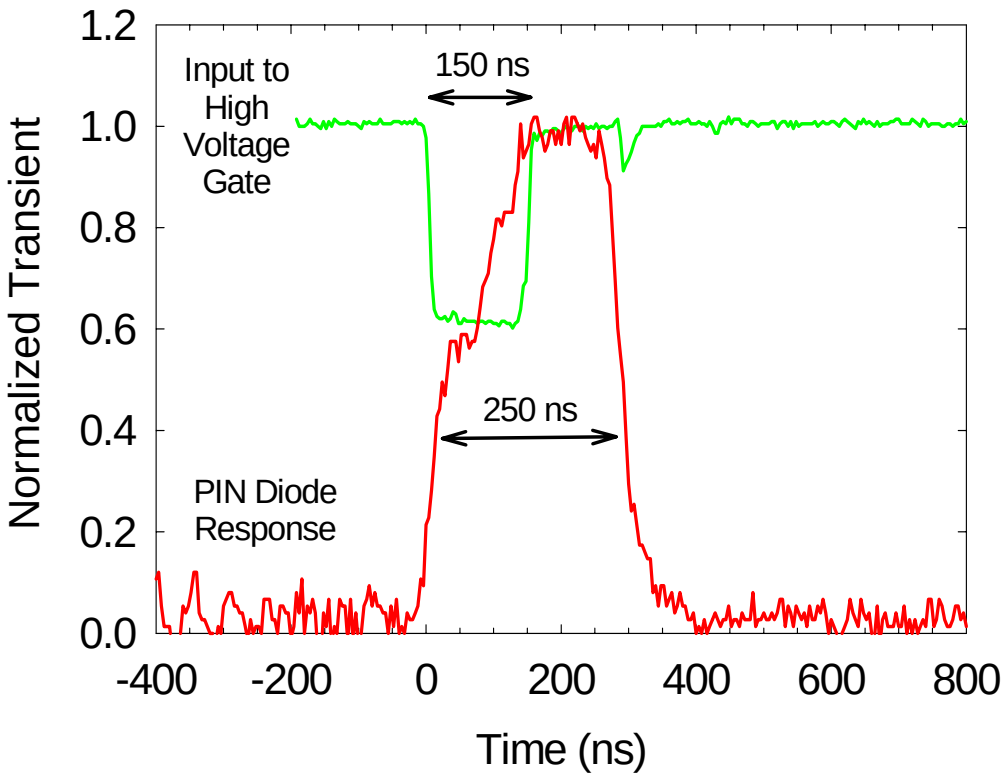

Figure 10. Normalized input signal to high voltage gate that controls beam deflection plates, plotted with PIN diode response to the same beam pulse. Although the input signal has a duration of 150 ns, the beam pulsewidth is considerably larger, about 250 ns.

~250 ns is due to the slow rise and fall time of the high voltage switcher and to the finite beam size at the deflection plates.

As part of ongoing upgrades to the focused ion microbeam line, Sandia designed a new test chamber and contracted with Raith Inc. to have it built. This new "hybrid" chamber incorporated the nuclear microprobe, a front-viewing optical microscope, and a scanning electron microscope. The new chamber, called the Micro-ONE (for Optical, Nuclear, and Electron microscopy) was installed in late 2000, replacing the existing microbeam test chamber. The electronics comprising the TRM were installed shortly thereafter on this chamber. Features of the Micro-ONE system include 0.1-µm stage resolution and GDSII navigation software (allowing beam targeting based on the mask layout files for the DUT). The Micro-ONE chamber has sample chucks for both 8" wafers and up to 162-wire pinout ZIF sockets. Figures 11 and 12 show photographs of the Micro-ONE chamber in place on the microbeam line in the IBMRL. This is the beam chamber currently used for all TRM measurements.

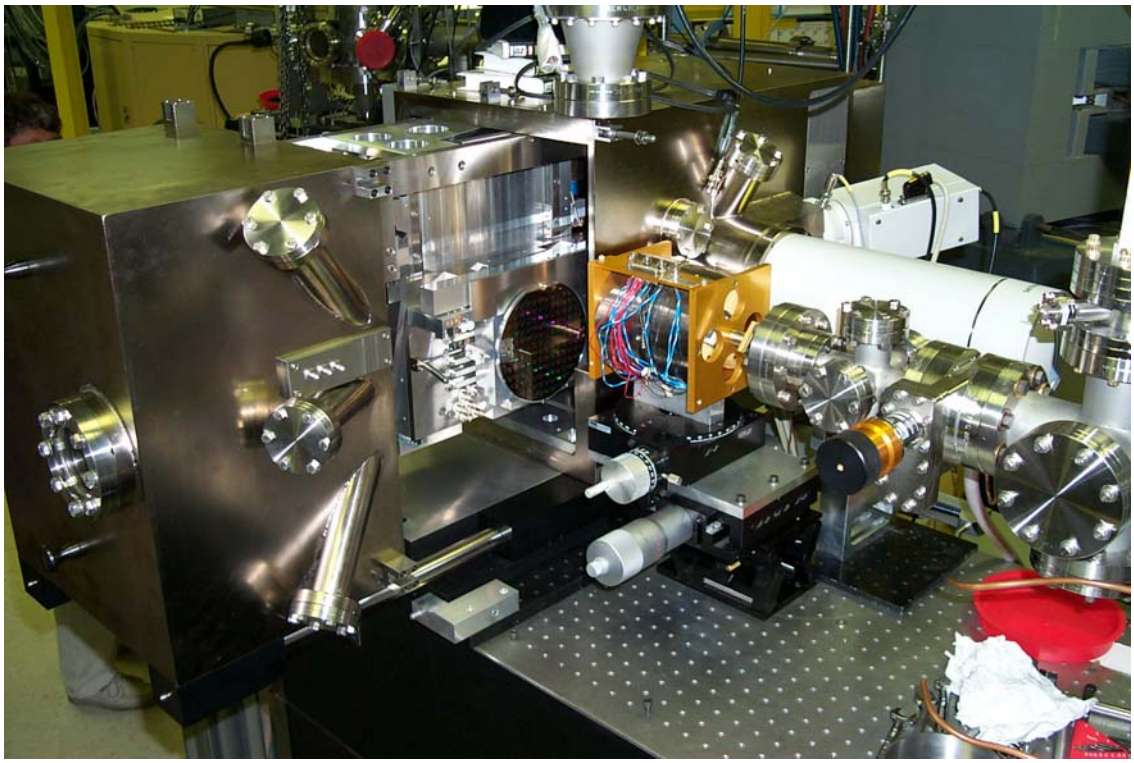

Figure 11. Micro-ONE beam chamber from back (upstream) side.

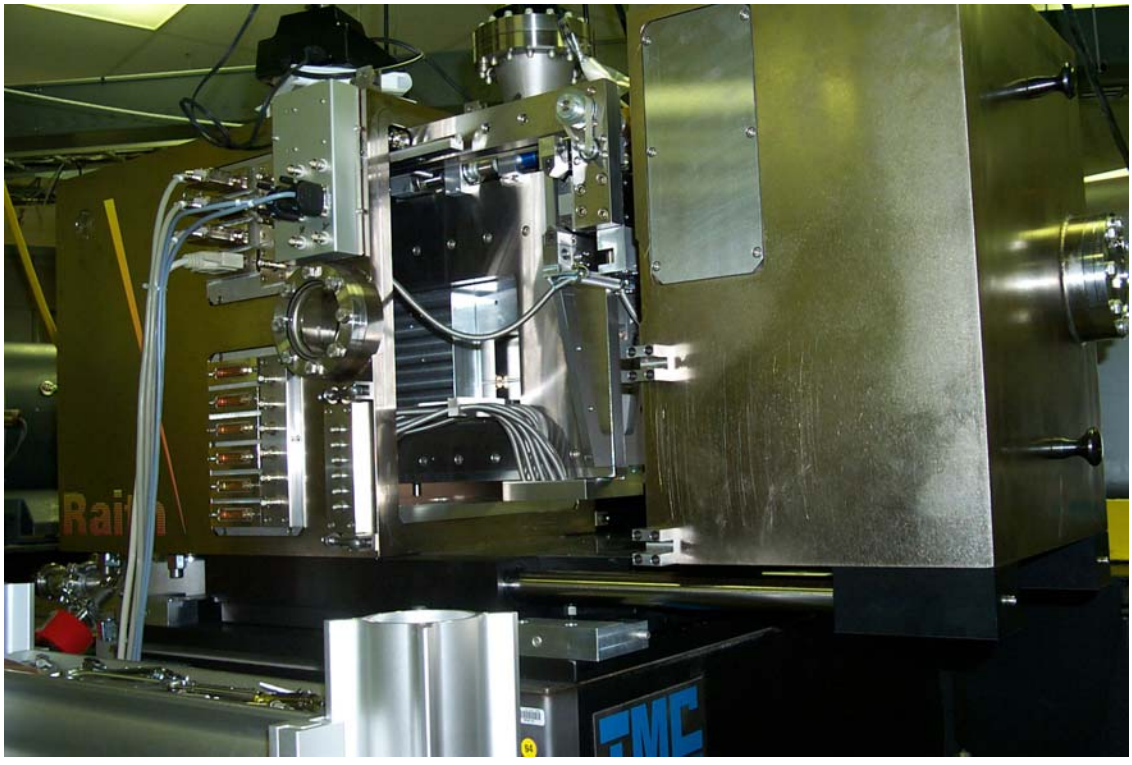

Figure 12. Micro-ONE beam chamber from front (downstream) side.

Physics of Dose-Rate Response in PIN Diodes

Experimental Details

Following the discovery of the unexpected storage time phenomenon observed in the initial TRM proof-of-concept experiments, we chose to continue experiments on the Hamamatsu S1223 PIN diode to determine the physical mechanisms responsible for the observed response [5]. The PIN diode has a large area (3.6 mm × 3.6 mm) and a deep intrinsic region (316.5 μm). A 25-V reverse bias was applied to the diode during the experiments using a bias tee circuit with a 2.9-kΩ resistor and a 12.3-nF capacitor. The transient response of the diode was measured using a DC-coupled oscilloscope with an input resistance of 50 Ω. For these experiments, a 35-MeV Cl^{+6} beam was used with a spot size of approximately 50 μm × 80 μm.

The beam pulse characteristics of the TRM system are difficult to measure. In a dose-rate source such as an electron linear accelerator (LINAC), a calibrated PIN diode is typically used to measure the duration and dose-rate of each pulse. Because the beam covers a large area and is not significantly attenuated by most materials, it is possible to obtain accurate *in situ* dosimetry at the same time that data is being collected on the device of interest. This is unfortunately not the case for the TRM system. Because the ion beam is focused to a small area and is attenuated by the DUT, it is not in general possible to simultaneously measure the characteristics of the beam pulse and collect data. The beam pulse characteristics must therefore be deduced indirectly.

For these experiments, the ion beam current measured by a Faraday cup just prior to delivering the beam pulse was used to calculate the equivalent dose rate for a given ion. The pulse duration is more difficult to measure. The pulsewidth is controlled by the duration of the gate signal input to the high-voltage deflection plates, but because of the finite response time of the high-voltage pulser and other delays in the system, the input gate signal is not an accurate representation of the actual beam pulse, as was discussed above and illustrated in Figure 10. At high dose rates, the presence of the charge storage phenomenon in the Hamamatsu PIN diode prevents us from using its response to directly deduce the beam pulsewidth. Because of this it was necessary to consider the beam pulsewidth as an adjustable parameter in the simulations, and the simulation results themselves were used to determine the probable pulsewidth for each exposure. We note here that it was actually the simulation results that first indicated a problem with the pulsewidth measurement, which was then confirmed by the experimental data.

Simulation Details

Three-dimensional simulations of the transient photocurrent response were performed using the Davinci mixed-level device/circuit simulator [2]. In the case of TRM experiments, it is necessary to model the dose-rate response in 3D, because the beam spot is incident on only a small area of the larger device. This leads to three-dimensional diffusion of charge throughout the device following the beam pulse. For these simulations the simulated device volume was 320 μm deep and 500 μm × 500 μm in the plane normal to the ion beam. Destructive construction analysis was performed to determine the doping profiles within the device to

facilitate device-level modeling of the diode. The same biasing circuit and oscilloscope resistance present in the experiments was included in the Davinci photocurrent simulations.

Mark II Transient Radiation Microscope Results

High Dose-Rate Results

Figure 13 shows TRM data for 10 successive exposures using a Cl^{+6} beam producing a calculated dose rate of 9×10^{10} rad(Si)/s. As previously noted, accumulated displacement damage from the ions degrades the measured photocurrent response, in this case by about 10% after ten 150 ns pulses. This damage in general may limit the number of exposures to which a part can be subjected before the onset of significant degradation, and precludes the use of the TRM for nondestructive dose-rate screening of parts. In these experiments we simply moved the ion beam to a new, undamaged region of the large diode before each exposure. For smaller devices or selective irradiation of a small area of a larger IC, it may be necessary to irradiate multiple DUTs to completely characterize a part's transient radiation response.

The photocurrent responses shown in Figure 13 were obtained using a beam pulsewidth of ~150 ns. Note that the measured signal persists beyond 1 μs, long after the radiation pulse is over. This is shown more clearly in Figure 14, which replots the data from just the first shot,

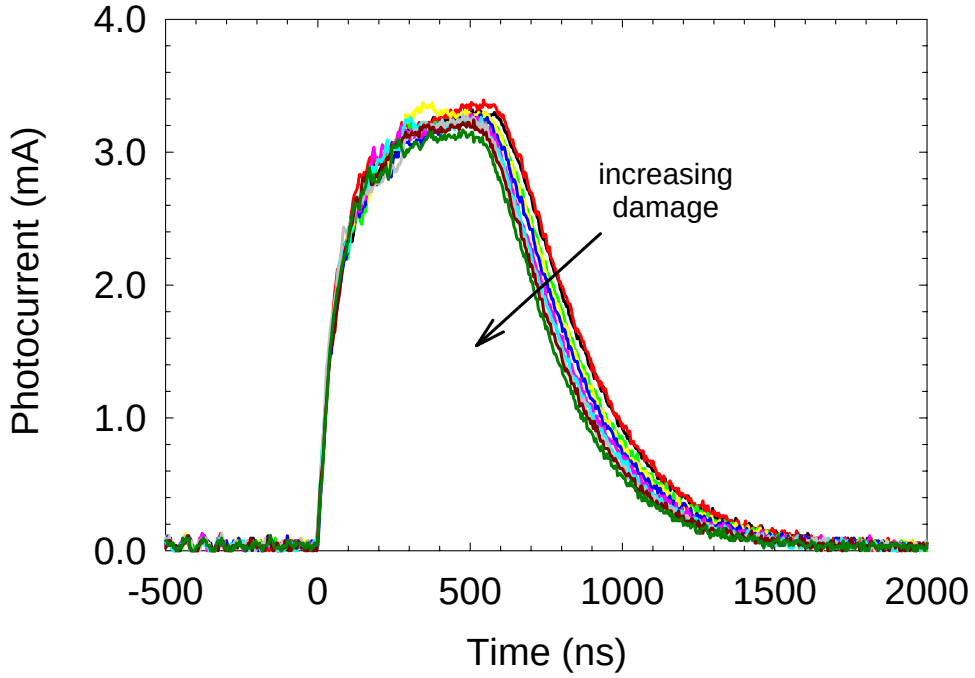

Figure 13. Measured photocurrent response of a Hamamatsu PIN diode following multiple 9×10^{10} rad(Si)/s 150-ns dose-rate pulses of 35-MeV Cl ions. Increasing damage from successive irradiations leads to about a 10% degradation in transient response after 10 beam pulses.

and the shaded region denotes the duration of the ion beam pulse. Surprisingly, the current in the diode continues to increase for several hundred nanoseconds after the ion beam pulse is over. This extremely long storage time is similar to that observed in the initial experiments. This storage time effect is *not* due to diode saturation (i.e., de-biasing because of the oscilloscope load resistance), which can also lead to increased photocurrent response duration [6]. Note that the current continues to increase after the pulse has ended, which is not typical of diode saturation. Also, because we are only irradiating a small volume of the diode, the photocurrent is only ~3 mA, which leads to a minimal drop in the bias voltage of about 150 mV (out of 25 V applied) across the diode.

Also shown in Figure 14 is the photocurrent response predicted by Davinci numerical device simulations. The Davinci simulations agree remarkably well with the measured response, and in fact predict the enhanced storage time of the PIN diode. The simulation results contain detailed physical information on the internal operation of the device, and can be studied to determine the cause of the enhanced storage time.

Figure 15 shows the simulated internal electrostatic potential distribution inside the diode immediately before and after the dose-rate pulse. The pictured volume is 500 μm (W) × 500 μm (L) × 320 μm (D). At time = 0, the electrostatic potential changes only in the depletion region (as expected), and a zero-field region exists below. Note that only the top 50-60 μm of the intrinsic layer are depleted in this diode at 25 V. At time = 250 ns the carriers induced by the dose-rate pulse have perturbed the majority carrier concentration in the diode,

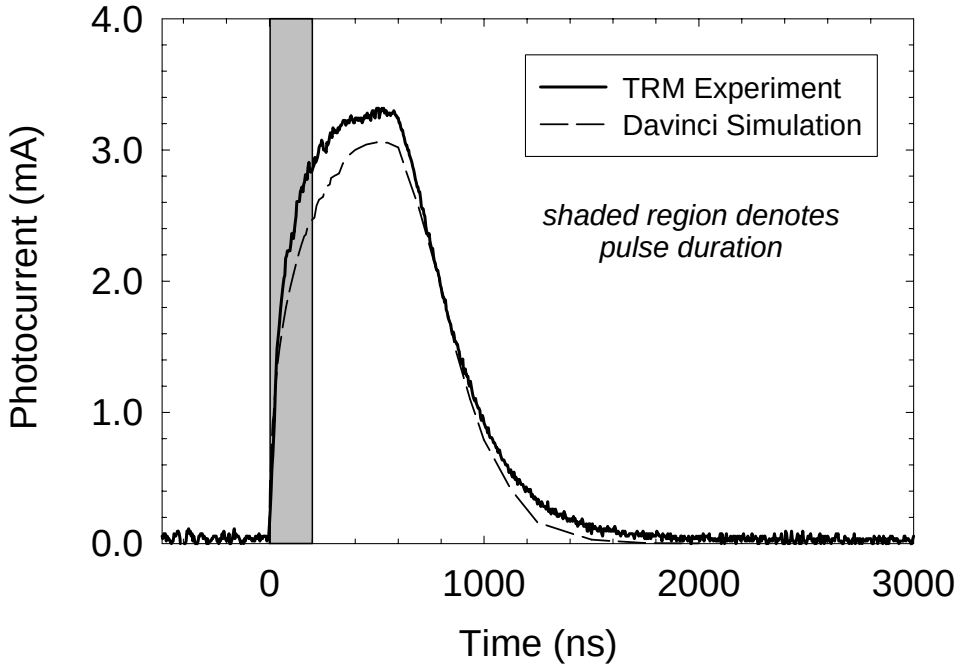

Figure 14. Measured and simulated photocurrent response of a PIN diode following a 9×10^{10} rad(Si)/s 150-ns dose-rate pulse. The device photocurrent continues to increase several hundred nanoseconds after the end of the dose-rate pulse. Davinci calculations predict this enhanced storage time.

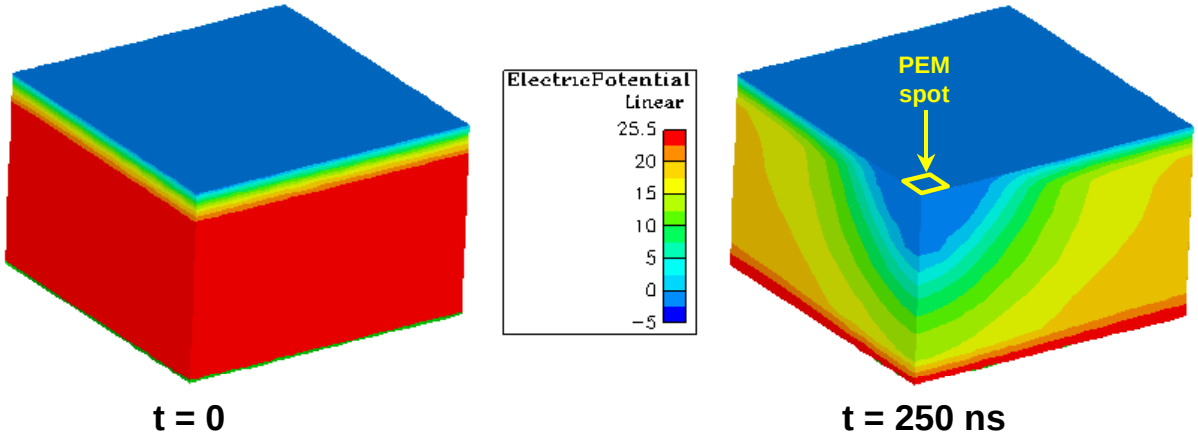

Figure 15. Electrostatic potential (in volts) in a PIN diode immediately preceding (t = 0) and following (t = 250 ns) a 9×10^{10} rad(Si)/s dose-rate pulse of 35-MeV Cl ions. The pictured volume is 500 µm (W) × 500 µm (L) × 320 µm (D). Note the dose-rate induced funnel and non-zero electric field (gradient of potential) deep in the device following the pulse.

and the potential contours are disturbed throughout the diode. This pushes the electric field deep into the device, and a field-free region now exists near the top of the device where the induced carriers are located. This is exactly analogous to the phenomenon of "funneling" that occurs following a single ion strike, and that contributes to single-event upset in microelectronics [7,8]. In the present case, the TRM beam spot just looks like an ion strike with a *very large* lateral extent.

After the pulse ends, the carriers diffuse and recombine throughout the diode, and the electrostatic potential slowly relaxes to its equilibrium (t = 0) state. As the potential relaxes, the electric field region "sweeps" up through the device, collecting the radiation-induced charge. Because this carrier diffusion and recombination occurs on a microsecond time scale, an enhanced storage time is observed in the photocurrent response. This effect is related to but distinct from past work, where electric field modulation due to perturbed majority carrier concentrations (a.k.a. conductivity modulation) has been observed to delay the transient photocurrent response in semiconductor junctions [9,10]. In this previous work the majority carrier concentrations were disturbed throughout the devices, in contrast to the TRM experiment, where they are perturbed only in a relatively small volume of the diode. In both cases, however, the field perturbations lead to a separation of the induced charge from high-field regions. This separation basically insulates part of the charge from being collected quickly by drift, and results in long charge storage times as diffusion and recombination are required to restore the initial electric field profile.

The funneling mechanism observed here is basically a result of the fact that for short-range ions such as chlorine (range = ~10 µm), the charge generated by the TRM only reaches the top portion of the active device. If the radiation pulse generates charge throughout the entire 320 µm depth of the device (as it would using x-ray accelerators such as SPHINX, or electron linear accelerators such as the Crane LINAC), Davinci simulations predict no enhanced storage time, as illustrated in Figure 16. In this figure, the simulated photocurrent response of

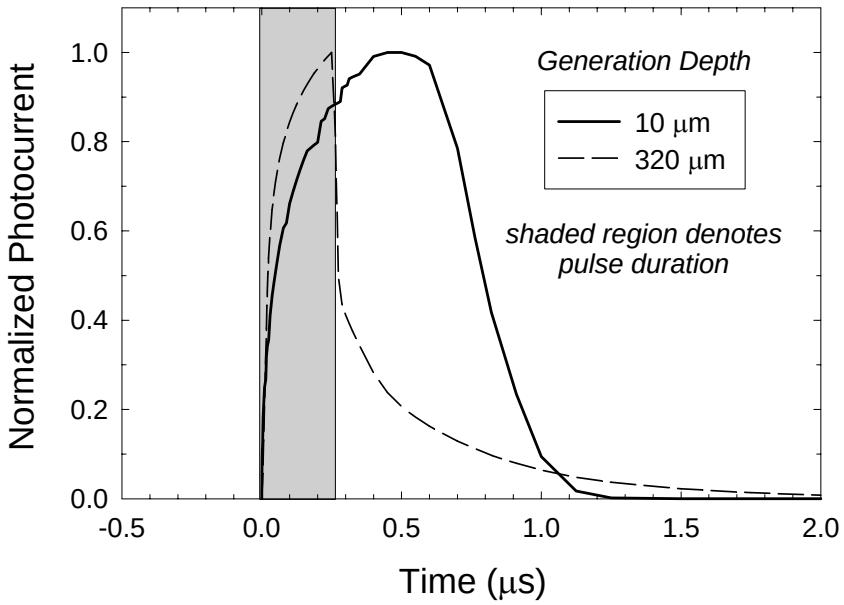

Figure 16. Simulated photocurrent response of Hamamatsu PIN diode for 1.2×10^{11} rad(Si)/s 250-ns dose-rate pulses with generation depths of 10 μm and 320 μm. The shaded region denotes the radiation pulse duration.

the Hamamatsu diode is plotted for two cases: beam spot charge generation limited to the top 10 μm of the device, and charge generation throughout the 320-μm deep diode. The simulated dose rate was 1.2×10^{11} rad(Si)/s, and the beam pulsewidth was 250 ns. For the case of charge generation throughout the device (dashed curve in Figure 16), the photocurrent response directly tracks the incident radiation pulse, with only a long diffusion tail after the pulse ends.

Lower Dose-Rate Results

We have performed further TRM experiments at lower dose rates using reduced ion beam currents. Figure 17 shows data from a 350-ns Cl^{+6} beam pulse with a dose rate of 9×10^{9} rad(Si)/s. It is clear that for this lower dose-rate pulse, the enhanced storage time is greatly reduced due to the smaller perturbation in the majority carrier concentration. As we go to even lower dose rates, the storage time phenomenon disappears completely, as shown in Figure 18 for a 2.4×10^{9} rad(Si)/s 250-ns pulse. The photocurrent response of the diode finally tracks the incident radiation pulse shape, indicating that the majority carrier concentration is not perturbed by this lowest dose rate irradiation. As described above and in [1], the lowest dose rate that can be used in the TRM system is limited by noise in the measured DUT photocurrent response and the accuracy with which the ion beam current can be measured. Note that in the Mk II system the DUT photocurrent noise has been reduced to < 0.1 mA, as evidenced by the lack of excessive noise in Figure 18.

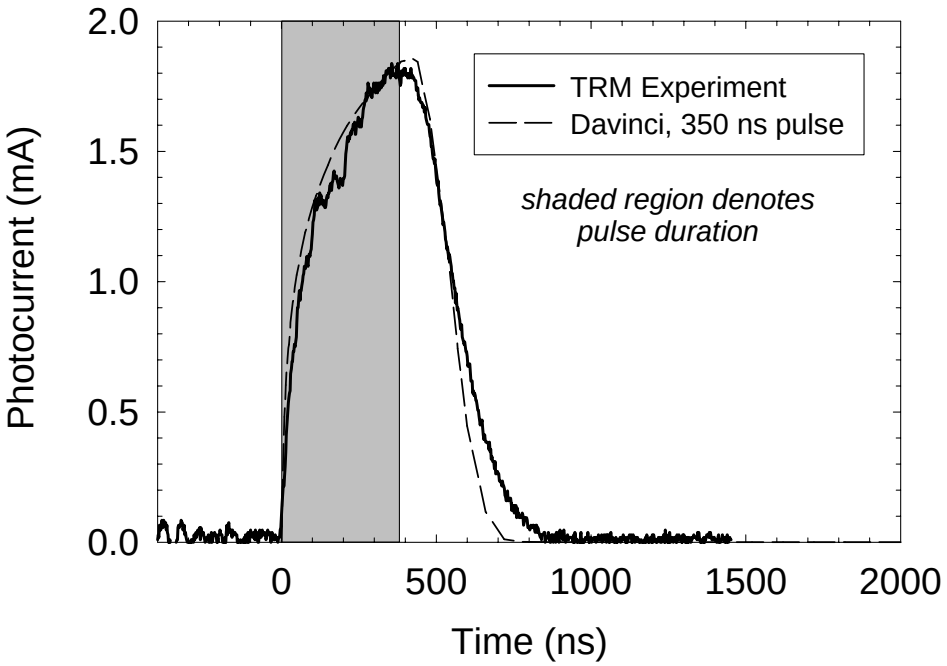

Figure 17. Measured and simulated photocurrent response of a PIN diode following a 9×10^{9} rad(Si)/s 350-ns dose-rate pulse.

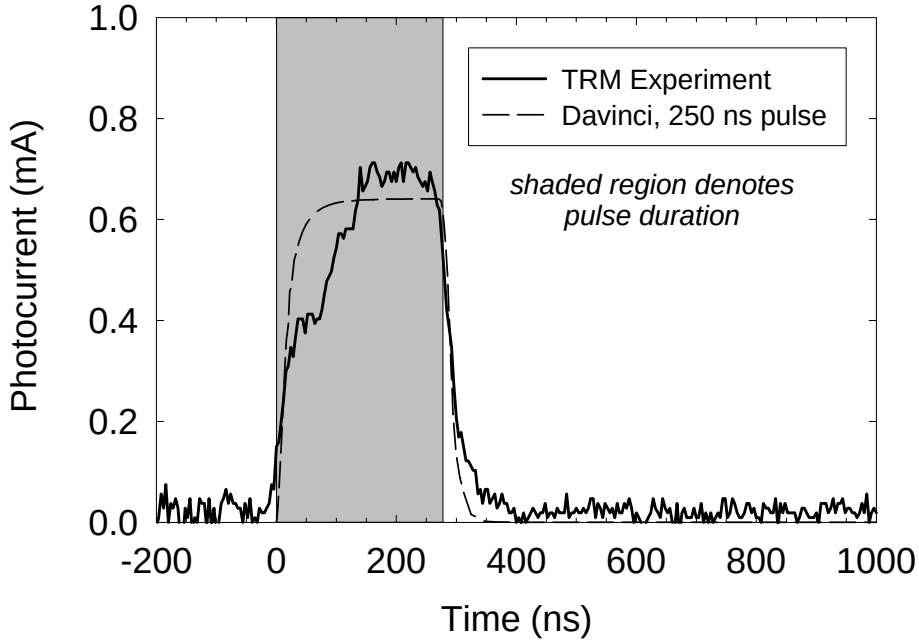

Figure 18. Measured and simulated photocurrent response of a PIN diode following a 2.4×10^{9} rad(Si)/s 250-ns dose-rate pulse. At this dose-rate, the photocurrent response tracks the beam pulse.

Sensitivity Study: Physical Model Parameters

Although the Hamamatsu PIN diode is not an ideal device for exploring the capability of the TRM system compared to more conventional dose-rate sources, it is a very good vehicle for Davinci simulation validation studies. For example, the ability of Davinci to predict the diode's unusual transient response behavior is encouraging and suggests that the current models in Davinci are adequate for dose-rate simulations.

We have also performed studies on the sensitivity of the PIN diode simulation results to the physical parameters used by Davinci. The simulation results shown in all of the figures to this point were obtained by using a minority carrier lifetime in Davinci of 1 μs (well within the normal range of values [11]). Because the field perturbation (funnel) relaxes only after the carrier densities fall below the background doping concentration in the diode, the enhanced storage time is extremely sensitive to minority carrier recombination lifetime. Figure 19 shows the sensitivity of the simulation results to minority carrier lifetime, where we have plotted the calculated photocurrent response waveforms for the same conditions as in Figure 14 for lifetimes from 0.2 μs to 1 μs. Relatively small differences in the minority carrier lifetime can produce large changes in the enhanced storage time as well as affecting the peak photocurrent. For the Hamamatsu diode, we find that a minority carrier lifetime of 1 μs produces the best results in comparison to the experimental data. As shown in Figures 17 and 18, this lifetime also produces accurate simulation results for the lower dose-rate experiments.

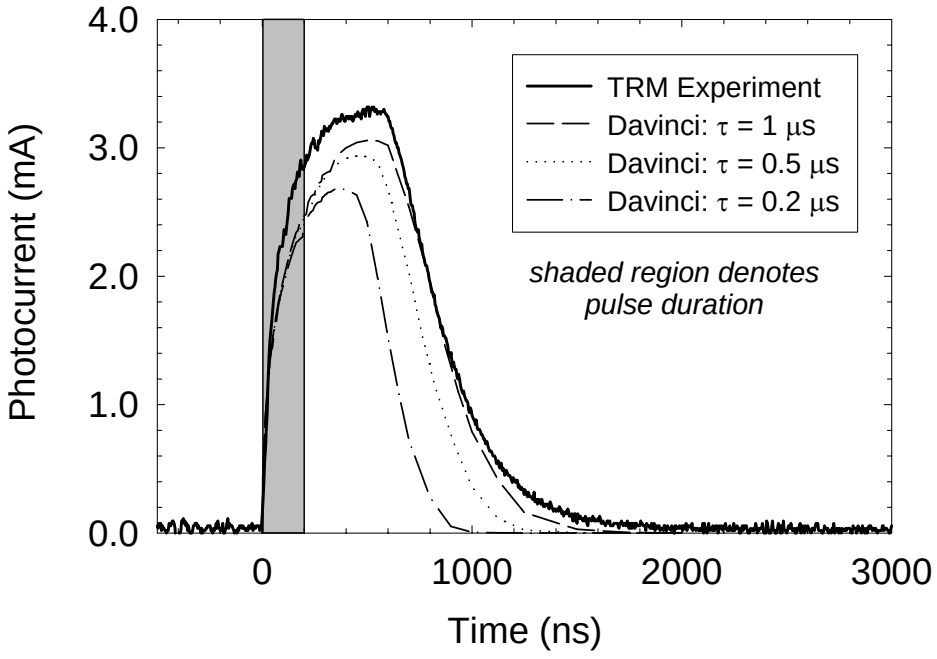

Figure 19. Minority carrier lifetime sensitivity of calculated PIN diode photocurrent response following a 9×10^{10} rad(Si)/s 150-ns dose-rate pulse.

The good agreement with data shown by these simulations suggests that, at least for the Hamamatsu diode, the information gleaned from construction analysis can be sufficient for accurate simulations. This has important implications for the modeling of the dose-rate response of commercial devices, since it is usually difficult to acquire detailed information on the device construction from the manufacturer. It must be noted, however, that this PIN diode is a very simple (almost one-dimensional) device. It remains to be seen whether sufficient information can be obtained from construction analysis to satisfactorily model more complex devices, although preliminary data indicate that it is possible at least for discrete transistors.

Comparison to Linear Accelerator Experiments

To further study the transient response of the Hamamatsu PIN diode and to further validate the Davinci simulator for dose-rate modeling, we performed linear accelerator (LINAC) experiments to complement the TRM data. For these experiments we used the 40-MeV electron LINAC at the Naval Surface Warfare Center in Crane, IN, and the 18-MeV electron LINAC at the Idaho Accelerator Center in Pocatello, ID. The diodes were again reverse-biased at 25 V using the same bias-tee configuration, and the pulsewidth was 10 ns for the Crane LINAC, and 25 ns for the 18-MeV Idaho LINAC.

No enhanced storage time effects were seen in any of the LINAC data, which covered dose rates from 10^4 rad(Si)/s to above 10^{10} rad(Si)/s. From the simulations of Figure 16, this is what we would expect because the LINAC generates charge throughout the entire depth of the device. Unfortunately, it is difficult to draw direct comparisons between the TRM data and LINAC data at high dose rates, because above about 5×10^7 rad(Si)/s, the diode response saturates in the LINAC experiments due to its very large area and relatively small (25 V) reverse bias. This is one advantage of the TRM system, in that very high dose rates can be achieved without saturation.

Figure 20 shows a comparison between Davinci simulations and LINAC data for a dose rate of 10^8 rad(Si)/s. Because the charge generation is now uniform throughout the entire device, the simulation was quasi-one-dimensional and scaled to the known diode die size. A minority carrier lifetime of 1 μs was used for these simulations. The simulations agree well with the data, but the simulated current falls off a little faster than the measured response. This slight discrepancy is at least partly due to the fact that the simulation assumed a perfect 10-ns step function dose-rate pulse, where the real pulse has a finite rise and fall time.

The peak photocurrent in the Hamamatsu diode as a function of dose rate is plotted in Figure 21. Data are shown for each of the LINAC facilities, as well as Davinci simulations with and without including the bias-tee and 50-Ω scope measurement circuit. The pulsewidth for the simulations was 25 ns, for the Crane data it was 10 ns, and for the Idaho data it was 25 ns. Also shown are the TRM data scaled to the full die area of the diode; for these data the pulsewidth varied from 150-350 ns. From Figure 21 we see that the Davinci simulations accurately predict the measured peak photocurrent over 6 orders of magnitude in dose rate, as well as correctly predicting the onset of saturation. A powerful feature of the simulations is the fact that we can remove the circuit load and calculate the intrinsic response of the unloaded diode attached to an infinitely stiff power supply. Such a capability allows one to construct a model for the intrinsic response of the diode that can then be imbedded in an arbitrary circuit to determine the circuit's transient response. This is difficult to do with empiri-

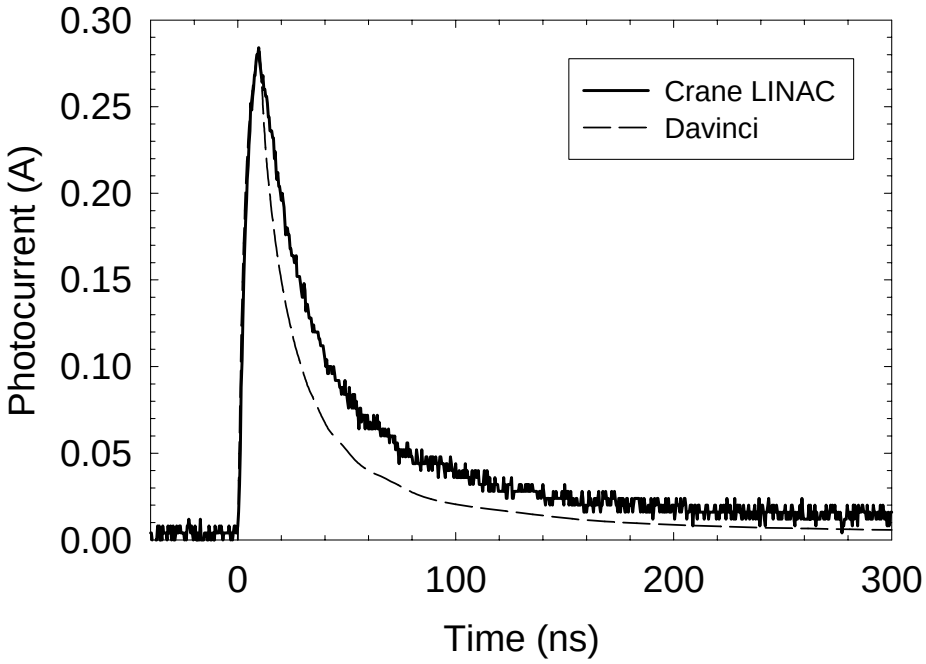

Figure 20. Measured and simulated photocurrent response of a PIN diode following a 10^8 rad(Si)/s 10-ns LINAC pulse.

cally derived transient response models, because they already include the impact of the measurement circuit used to obtain the data on which the model is based. Note that because the impact of the measurement circuit is greatly reduced in TRM experiments, the TRM data should approach the unloaded Davinci simulations. In the case of this PIN diode, they fall below the unloaded simulation predictions because the limited range of Cl ions in silicon results in much less total charge generation for the TRM experiment compared to the LINAC experiments.

Discussion

The Davinci 3D simulation results are in good agreement with both TRM and LINAC data taken over many orders of magnitude in dose rate. These results indicate that the physical models used in device simulators are capable of accurately predicting dose-rate response at the device level. The simulated photocurrent response of the PIN diode is very sensitive to the minority carrier lifetimes in the device, but reasonable values produce a good match to experimental data. To produce conservative results for a device for which the minority carrier lifetimes are not known, it seems reasonable to assume a value of 1 μs.

The results shown here indicate that for devices sensitive to deep charge collection such as these PIN diodes, the TRM system cannot accurately simulate the photocurrent response that would be obtained from x-ray or electron irradiators. Fortunately, many devices of interest to systems are planar devices in which only the top portion of the device is active, for example

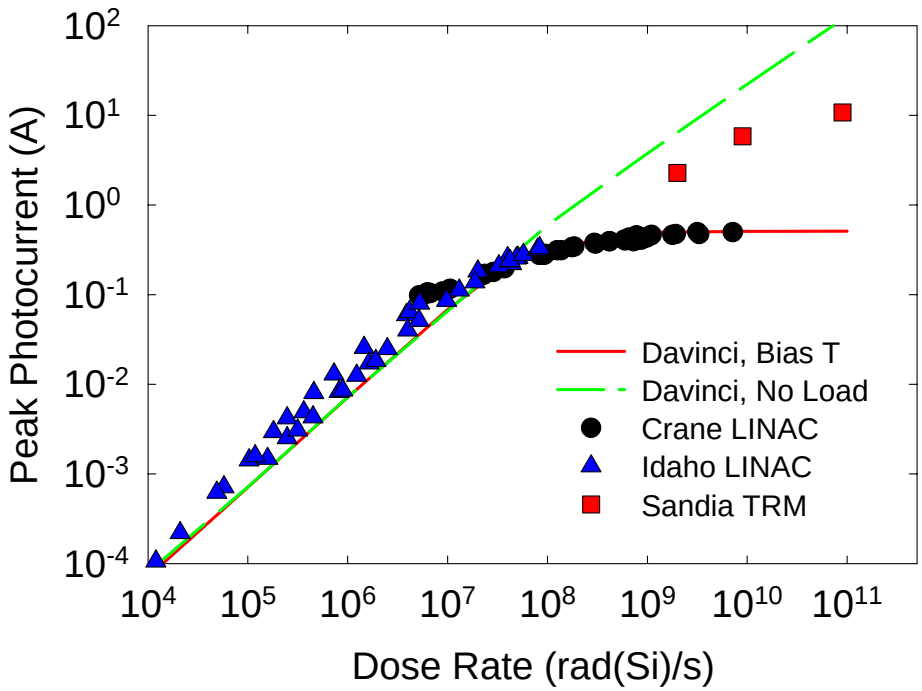

Figure 21. Peak diode photocurrent as a function of dose rate for LINAC experiments and simulations. Also shown are TRM data scaled to the full die area.

devices fabricated on thin epitaxial substrates or using silicon-on-insulator (SOI) technology. Results for other device types will be discussed shortly. The limited range of photogeneration produced by heavy ions is not expected to be a serious shortcoming of the TRM system for these devices. Devices built on bulk or thick epitaxial substrates may still present a challenge, as may advanced technologies with many levels of metallization or thick passivation overlayers, particularly if high dose rate irradiations are required. A further limitation of the TRM is that because the beam spot irradiates only a small cross-sectional area of the device, it cannot directly address large-area effects such as rail-span collapse that result from global photocurrent in an IC [12].

Despite these limitations, the TRM system is an excellent tool for model validation, allowing precisely controlled dose-rate experimentation at the microscopic level. The resulting data are key to validating physical models to enable truly predictive dose-rate simulations. In addition to providing transient radiation data to which device-level simulations can be directly compared, the TRM can be used to study localized photocurrents in an IC. For example, if a particular subcircuit were suspected to be limiting the overall transient radiation hardness of an IC, it could be directly studied using the TRM. Such a capability has proven itself to be very valuable for diagnosing single-event upset vulnerabilities, and will be a unique advantage of the TRM for improving the transient radiation response of ICs.

Further Developments: Higher Dose Rates and Shorter Pulses

The Mark III TRM

Originally we planned to achieve shorter pulses by using a faster high-voltage pulser or by pulsing the ion source. Both methods are expensive and the second one is very complicated. We found a simpler and cheaper way to achieve 20 ns pulses and calculations indicated that we would be able to reduce the pulsewidth even further to below 10 ns. Instead of sweeping the beam onto the target, keeping it on, and then sweeping off, we sweep the beam past an aperture in front of the DUT. This way the pulse length is determined by the speed of the deflection voltage change speed (rise time of the pulser) and the size of the beam when it enters the deflection plates. This change was implemented in the Mk III TRM, and with a beam size of approximately equal to the gap between the deflection plates we achieved a beam pulse of about 20 ns full-width half-maximum. Photocurrent responses in a Hamamatsu PIN diode are shown in Figure 22 for dose rates from 3.7×10^{9} to 1.26×10^{11} rad(Si)/s. In the figure we can see that the diode response is riding on a larger noise signal that is probably due to the deflector itself. The figure clearly shows the extended storage time for larger dose rates.

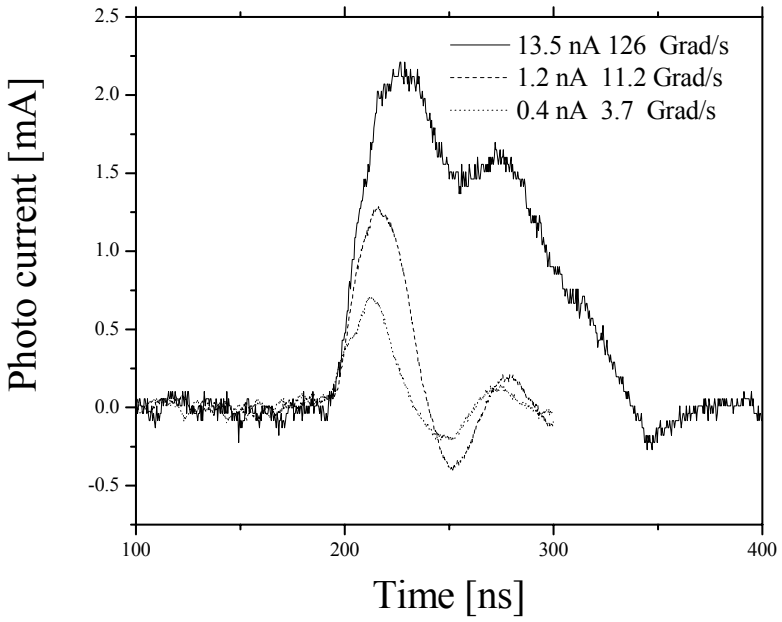

Figure 22. Hamamatsu PIN diode photocurrent responses for 20 ns beam pulse at various dose rates. For this experiment, the Mk III TRM was configured to sweep the ion beam past an aperture in front of the DUT.

Determining the Dose Rate and Beam Spot Size

Determining the exact dose rate provided by the TRM remains a challenging task, as is quantifying the size of the TRM beam spot on the DUT. As mentioned earlier, dosimetry at broadbeam facilities is performed simultaneous to the irradiation, so that the dosimetry accurately reflects the actual pulse obtained during the experiment. In the TRM, this is not possible, and the ion beam current must be read immediately before and after the irradiation using a Faraday cup. Unfortunately, the ion beam current fluctuates to some degree, and even if we read it immediately before the shot, it might not be the same during the shot. In addition, the beam spot size measurement is difficult, and directly impacts the calculated dose rate. Typically we determine the beam spot size by irradiating a piece of glass and recording the optical image in a BMP file, and then we calculate the size from the image. The problem is that the beam spot might be smaller than the area from which light is emitted. Also, there is always some background emission and the center of the beam spot image is frequently saturated, so we have no measure of the relative intensity in the beam center.

Figure 23 shows examples of the beam spot image from a 20-MeV carbon ion TRM experiment. The central white part is where the intensity is saturated; it can be seen clearly also on the surface plot. This makes the spot size determination a bit difficult. If we calculate every point above the background, we find a beam spot area of 13,983 μm^2, but if we count only points above 50% of the saturation level then we get 7060 μm^2, counting only points above 90% of the saturation level the result is 4058 μm^2, and counting only the points at the saturation level gives 3644 μm^2. So the question is which area to use? In reality, we probably need to consider the full area but take into account that there is a dose-rate distribution across the beam spot. If the photocurrent were linearly proportional to the dose rate (which is linearly proportional to the beam current density) we could calculate the photocurrent for every point and just add it up. Unfortunately, there is not always a linear relationship between the dose rate and the induced photocurrent.

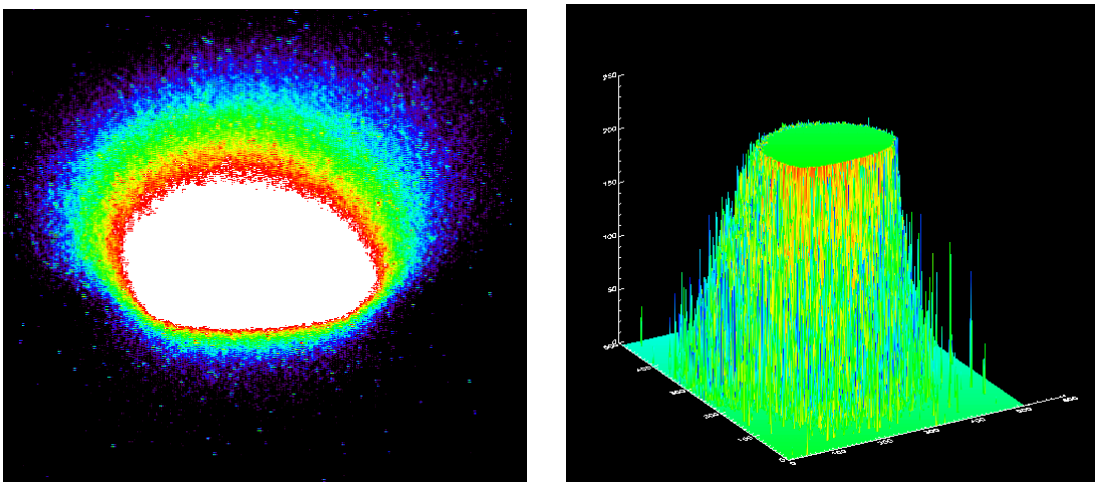

Figure 23. False-color and surface plots of ion beam intensity for a 20-MeV carbon ion TRM irradiation.

Thin PIN Diode Experiments

Storage Time Effects

To test whether the TRM ion range limitation was indeed responsible for the PIN diode storage time phenomenon as predicted by Davinci, we obtained some thin (15 µm intrinsic region layer thickness) and thick (50 µm intrinsic region layer thickness) PIN diodes manufactured by Emerge Corporation. We performed TRM measurements on the two Emerge diodes as well as the original Hamamatsu diodes. 20-MeV carbon ions were used for the experiments, providing dose rates from 1.2–9.0×10^9 rad(Si)/s.

We observed basically three different kinds of waveforms, as illustrated in Figures 24-26 (note that all three figures have the same scales):

1) The photocurrent is present only during the beam pulse. The waveforms from the thin Emerge diodes at high biases are like this (Figure 24).

2) The photocurrent increases during the beam pulse and exponentially decreases after the beam is turned off (Figure 25). In this case there is no storage time, but the bias voltage is not enough to completely deplete the diode. These waveforms are observed for all three diodes at low dose rates and low biases, and at higher dose rates for the thin Emerge diode when it is not fully depleted.

3) The photocurrent grows even after the beam is switched off (Figure 26). After reaching some maximum, it decreases exponentially. This is the well-known storage time effect, and both the Hamamatsu and the thick Emerge diode show it, but the thin Emerge diode does not.

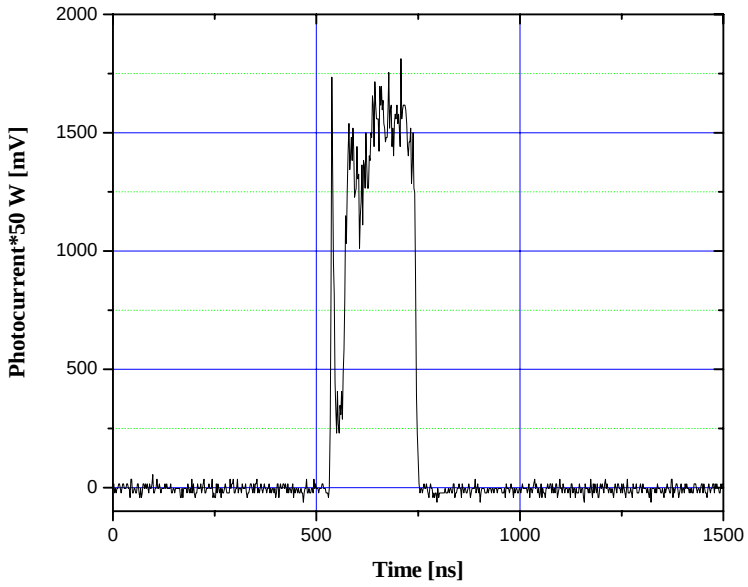

Figure 24. Photocurrent response in a 15 µm Emerge diode at –50 V bias and a dose rate of 9×10^9 rad(Si)/s. The photocurrent transient tracks the 200 ns TRM pulse.

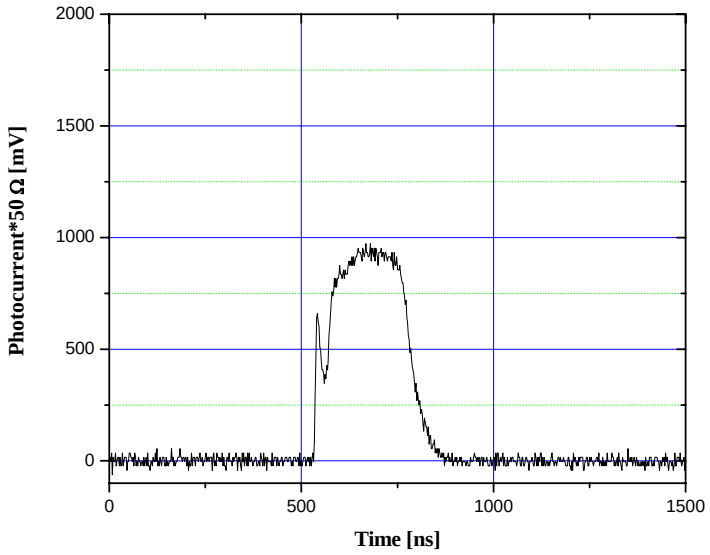

Figure 25. Example of a "type 2" response- Thin Emerge diode response at low bias showing diffusion tail.

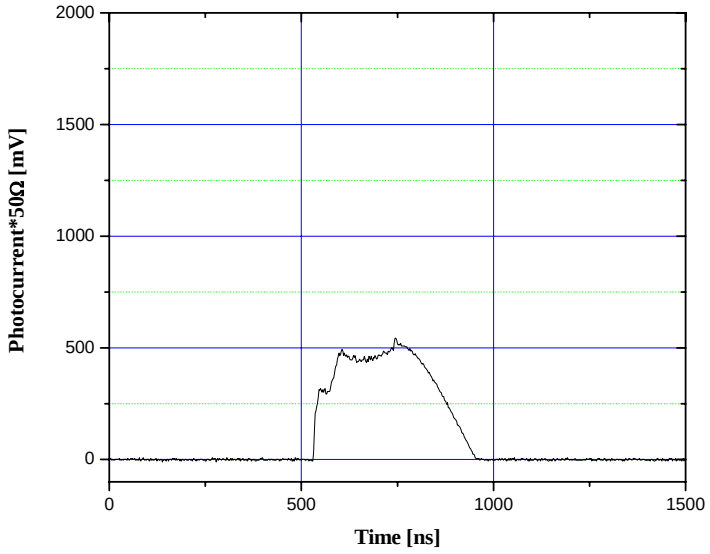

Figure 26. Example of a "type 3" response- Thick Emerge diode response at high dose rate showing storage time effect.

For 20-MeV carbon ions, the ion range (~15 μm) is just sufficient to penetrate through the intrinsic layer of the thin Emerge diode, so it never shows a storage time effect. On the other hand, the thick Emerge diode is much like the Hamamatsu diode, and it consequently shows a similar storage time. These experiments validated that Davinci correctly described the physical mechanism behind the storage time effect.

Transient Photocurrent Non-Linear Effects

Figures 27-29 compare and contrast the peak photocurrent response of the three PIN diodes. Note that for all of these figures, the peak photocurrent has been scaled up to the full diode area, although the TRM only irradiates a small spot. For the thin Emerge PIN diode, reverse biases greater than about –10 V are sufficient to fully deplete the intrinsic layer. For these biases, all charge deposited by the TRM pulse within the intrinsic layer is quickly collected, leading to a linear dependence of peak photocurrent with dose rate (Figure 27). Because the intrinsic layer is fully depleted there is only a slight bias dependence of the peak photocurrent at high reverse biases. As the bias is decreased below –10 V, the intrinsic layer is only partially depleted, leading to a sublinear dependence of peak photocurrent on dose rate.

Results for the thick Emerge diode are shown in Figure 28. For this device, the carbon ions do not fully penetrate the intrinsic layer, leading to the storage time effect at high dose rates. This effect spreads out the photocurrent response, leading to lower peak photocurrents at high dose rates. For this device, the photocurrent response is non-linear even at high reverse biases. Results for the Hamamatsu diode are similar to the thick Emerge diode (Figure 29), but the Hamamatsu diode shows an even more pronounced storage time effect and an even stronger dependence of peak photocurrent on the diode bias. This is shown more clearly in Figure 30, which plots the bias dependence of peak photocurrent in all three diodes at a dose rate of 20 Grad(Si)/s.

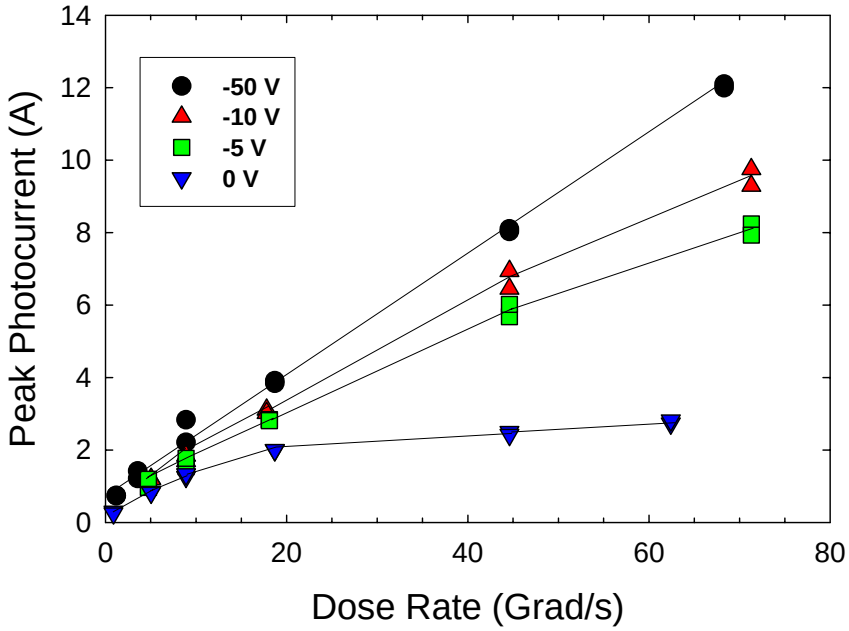

Figure 27. Peak photocurrent as a function of dose rate and bias condition in an Emerge PIN diode with 15-μm thick intrinsic layer.

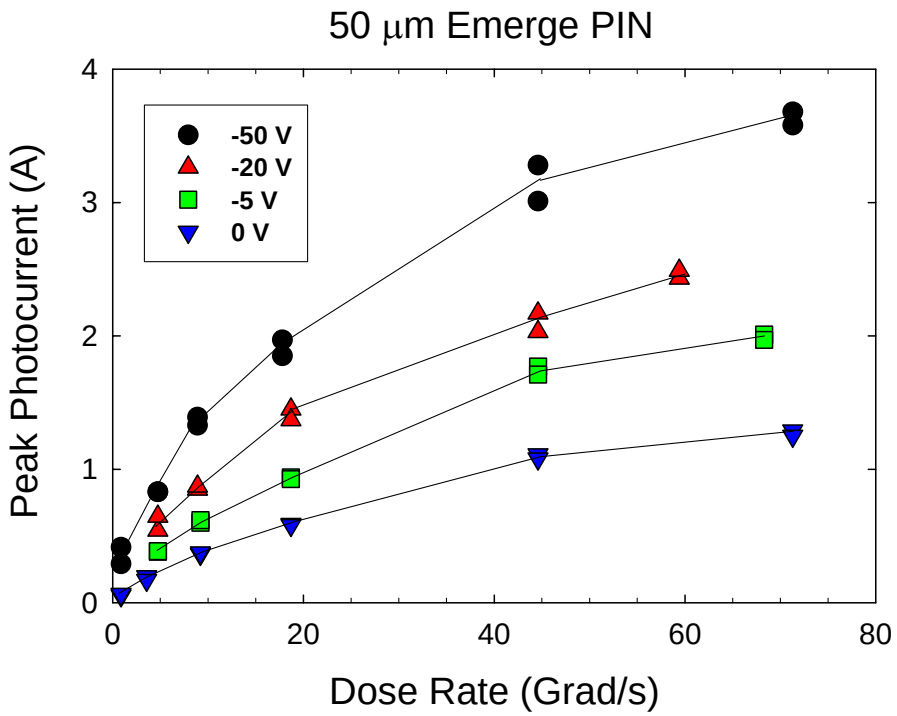

Figure 28. Peak photocurrent as a function of dose rate and bias condition in an Emerge PIN diode with 50-μm thick intrinsic layer.

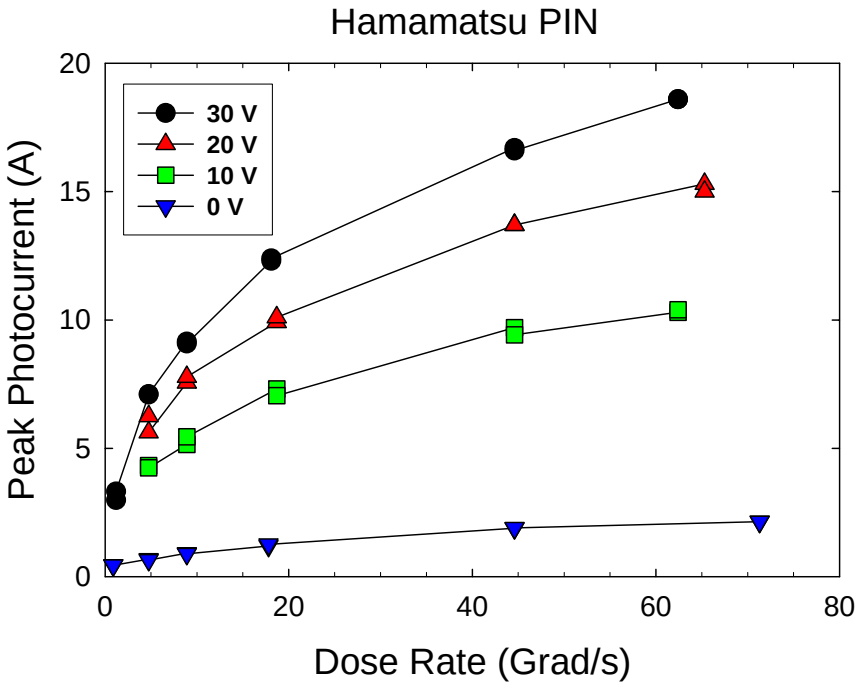

Figure 29. Peak photocurrent as a function of dose rate and bias condition in a Hamamatsu PIN diode.

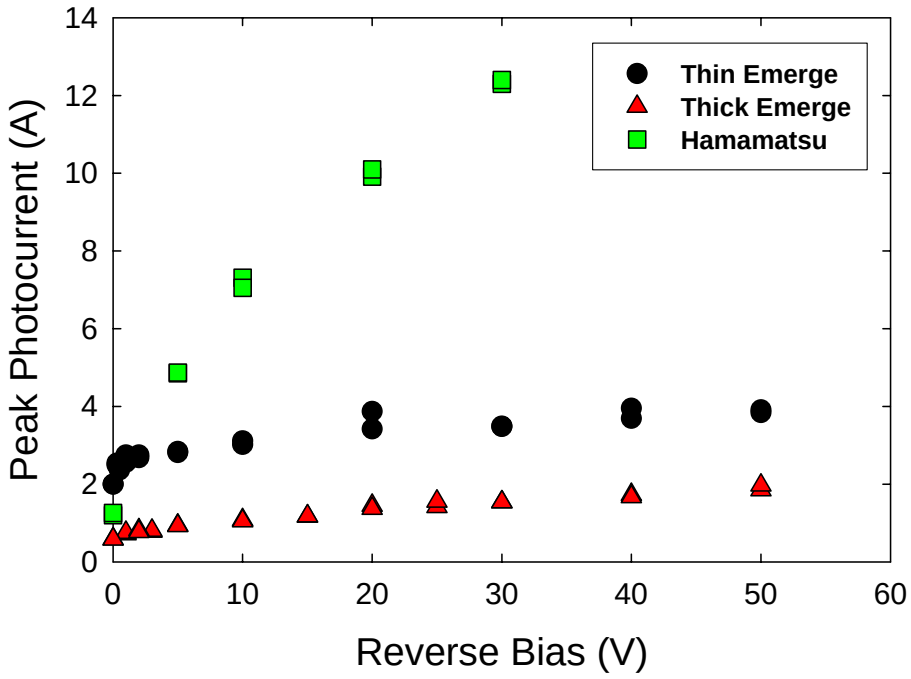

Figure 30. Peak photocurrent in PIN diodes as a function of bias condition at a dose rate of ~20 Grad(Si)/s.

Application of TRM to Bipolar and CMOS Devices

The Mark IV TRM

The "Mark IV" version of the TRM has been successfully set up and is now being used. This final version of the TRM can operate in either a short-pulse or a long-pulse mode. In the long-pulse mode, the ion beam is swept into the slits, stays there for from 250 ns to microseconds, and is then deflected away from the slits. In the short-pulse mode, the ion beam is swept from one side of the slits to the other side, passing through the slits only very briefly (~10 ns). In long-pulse mode we have been able to achieve dose rates in excess of 1 Trad/sec (10^{12} rad(Si)s). In short-pulse mode it is very difficult to precisely measure the dose rate (in addition to the complications previously noted), because the pulse contains so few ions. An additional complication is that because so few ions are contained in the pulse, the pulse reproducibility is poor. In future, non-LDRD-funded work it may be possible to further improve the system by using beam blanking directly on the ion source rather that controlling the accelerated beam. This method would have the further benefit of reducing beam noise at the end station.

To be a useful hardness assurance tool, it is essential that the TRM reproduce transient photocurrent results obtained in more usual broad-beam dose-rate sources such as flash x-ray machines or electron LINACs. While not typical of devices used in electronics systems, the PIN diode results were an excellent vehicle for studying the accuracy of the physical models

in Davinci. More typical devices and integrated circuits are fabricated with thin active device regions, and the ions used in the TRM are expected to have sufficient range to probe the entire sensitive charge collection volume.

Bipolar Transistor Experiments

2N2907 PNP Transistor

We tested 2N2907 pnp bipolar transistors being considered for system use in the TRM and compared the results to data taken at the electron LINACs at the Idaho State University Accelerator Center. The results are shown in Figure 31, which compares the TRM and LINAC data. Note that the TRM data have been adjusted for the transistor area, since the TRM does not irradiate the entire 2N2907 die area. The LINAC data cover a much larger range of dose rate than is possible in the TRM due to noise at low dose rates, but in the range where the measurements overlap, the TRM data agree well with the LINAC data. At high dose rates, the very large currents measured at the LINAC are limited by saturation, but the TRM results do not suffer from this problem. These data validate the use of the TRM as a dose-rate source that can emulate more traditional methods, at least for some devices.

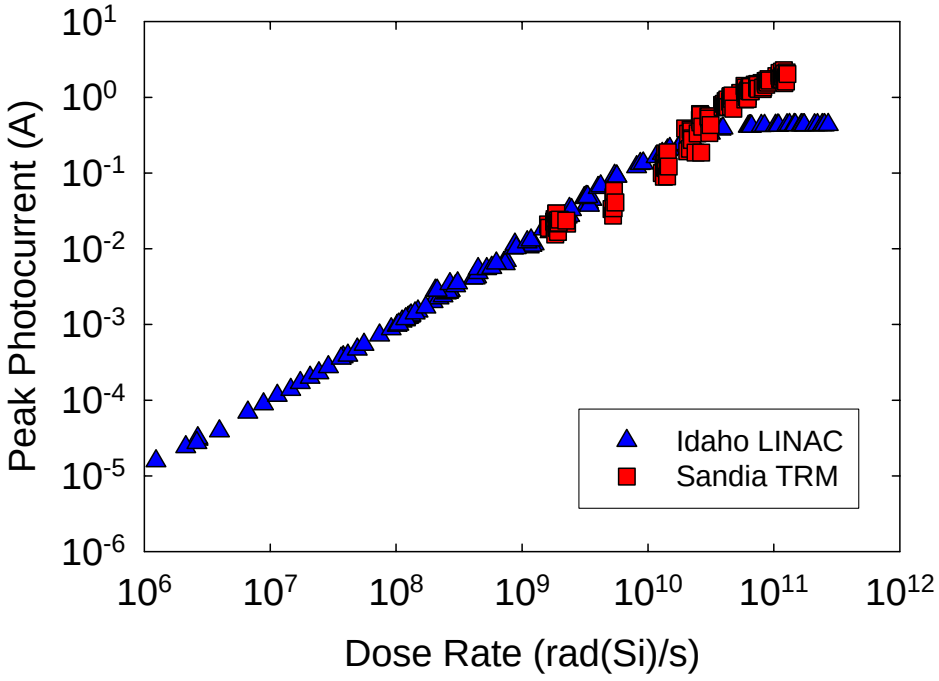

Figure 31. Comparison of peak photocurrent in a Motorola 2N2907 pnp bipolar transistor measured by TRM and at an electron linear accelerator. At high dose rates (>3×10^{10} rad(Si)/s) LINAC measurements are limited by saturation.

2N2222 NPN Transistor

In addition to the 2N2907 discrete pnp transistors, we also measured the TRM photocurrent response of 2N2222 discrete npn transistors being considered for system use. The response of the 2N2222 at high bias voltage is linear, in contrast to the 2N2907, which shows a slight superlinear behavior at high dose rates just before saturation. At high dose rates and 0 V bias the peak photocurrent becomes practically constant because diffusion dominates the charge collection process, while at high reverse bias the photocurrent continues to increase linearly.

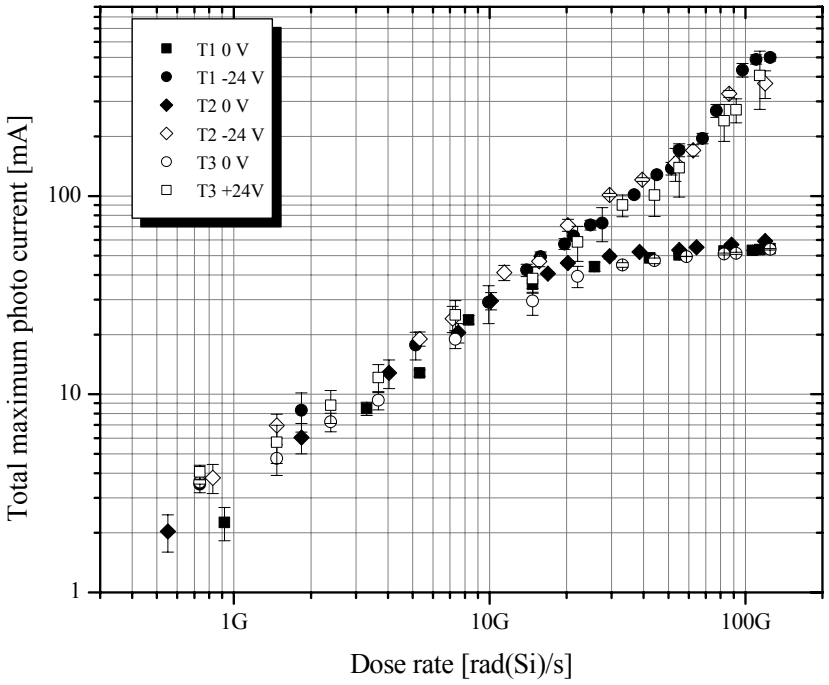

Figure 32. Peak photocurrent in 2N2222 npn bipolar transistors at -24 V and 0 V bias voltages.

CMOS Transistor Experiments

CMOS6r Transistors

TRM experiments were carried out on test transistor structures fabricated using SNL CMOS6r technology. For illustration, results on transistors on p-type substrate are shown in Figures 33 and 34. The photocurrent changes linearly with the dose rate since these structures have a thin active layer which is completely penetrated by the 35 MeV Cl beam. This is expected based on the previous experiments and simulations on PIN diode. Also, the photocurrent response scales with the size of the gate (and with the overall size of the transistor).

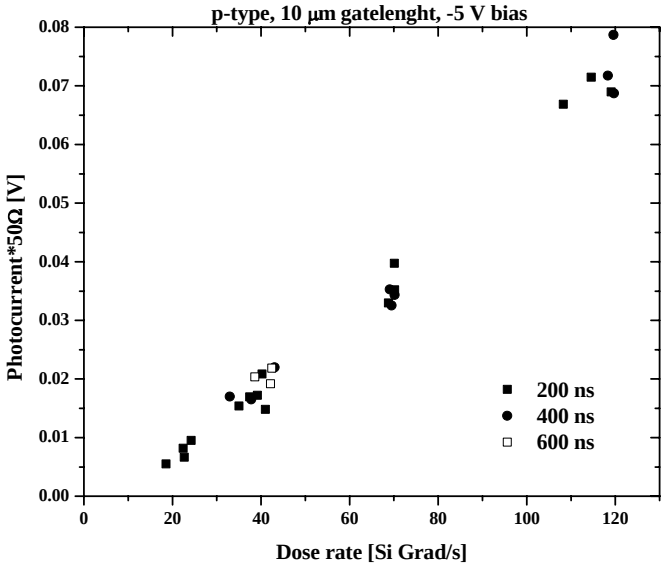

Figure 33. Photocurrent of 10 μm gate width transistor test structures on p-type substrate at different pulse lengths. The response is quite linear and it does not depend on the pulse length.

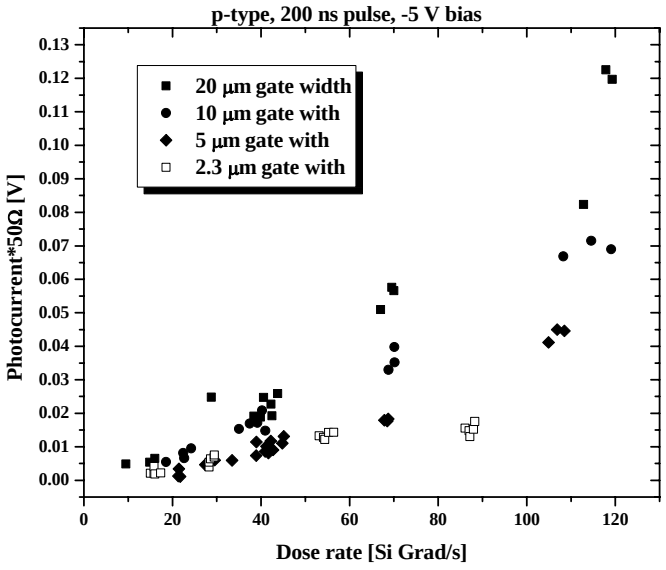

Figure 34. Photocurrent responses of transistor test structures with different gate widths at 200 ns pulse. The amount of photocurrent decreases with decreasing gate width as it was expected.

Conclusions

We have shown that the nuclear microprobe can be successfully used to simulate high dose rate events. Dose rates up to 10^{12} rad(Si)/s were achieved using high energy heavy ion beams focused to 50-100 μm diameter spots. Usually the beam pulse length was in the order of 200 ns and shorter pulse length was achieved although at somewhat lower dose rate. These experiments demonstrate that the nuclear microprobe can be successfully used to study the physical mechanisms of the high dose rate radiation response of microelectronic circuits. During the experiments we discovered an anomalous storage time in devices whose active region was not penetrated completely by the ion beam. This phenomenon was predicted by the Davinci device code. Our experiments on super thin PIN diodes confirmed the Davinci prediction that this phenomenon does not occur in thin devices where the ion beam completely penetrates the active region. This was a significant step in the validation of device codes to handle transient radiation effects in microelectronic devices.

After the first experiments on simple PIN diodes, TRM measurements were done on commercial and Sandia-fabricated parts. These results were compared to experimental results from linear accelerator facilities. The TRM has an advantage over the LINACs in that the photocurrent does not saturate at high doses as in the LINAC experiments. This allows checking the device codes without introducing external circuit loading effects.

The TRM has proved itself to be a useful addition to Sandia's radiation effects microscopy toolbox. In the future it will be routinely used to test various parts used in nuclear weapons. We intend to further improve the weak points of the method (e.g., current measurement, beam spot determination). Furthermore, we are planning to use shorter pulses routinely as we demonstrated. By using a new method (deflecting the beam at the ion source) we expect to have higher dose rates available with better control of the ion beam pulse. An important discovery during this work is the possibility that the TRM system may also be able to simulate reactor or weapons neutron damage effects in microelectronic devices, and this prospect is being further pursued.

Acknowledgements

We would like to thank Joe Polito for his strong support in the course of developing the Mark II TRM with the new Micro-ONE beam chamber. We also thank Jim Lee for additional RES support in extending the TRM capabilities to possible simulation of neutron effects and for supporting the LINAC experiments at Idaho State University.

References

[1] *The Sandia Nuclear Microprobe*, B.L. Doyle, N.D. Wing, Sandia Report SAND82-2393, (November 1982).

[2] Davinci 1999.2.0 (Avanti Corporation, 1999).

[3] P. E. Dodd, "Device simulation of charge collection and single-event upset," *IEEE Trans. Nuclear Science,* vol. 43, no. 2, pp. 561-575, Apr. 1996.

[4] S. N. Renfrow, W. Beezhold, P. E. Dodd, D. S. Walsh, and B. L. Doyle, "Device-level prompt photocurrent radiation microscopy using Sandia's ion microprobe facility," presented at the 18th Hardened Electronics and Radiation Technology Conference, Anaheim, CA, March 21-25, 2000, and accepted for publication in the *J. Rad. Eff. Res. Engnrg.,* vol. 19.

[5] P. E. Dodd, G. Vizkelethy, W. Beezhold, D. S. Walsh, M. R. Shaneyfelt, J. R. Schwank, and B. L. Doyle, "Device-level studies of dose-rate response using numerical simulations and transient radiation microscopy," presented at the 19th Hardened Electronics and Radiation Technology Conference, San Antonio, TX, March 6-9, 2001, and accepted for publication in the *J. Rad. Eff. Res. Engnrg.,* vol. 20.

[6] J. P. Raymond, "Analysis and Testing of Radiation-Induced Effects in Microcircuits," 1982 IEEE Nuclear and Space Radiation Effects Conference Short Course, Las Vegas, NV.

[7] C. M. Hsieh, P. C. Murley, and R. R. O'Brien, "A field-funneling effect on the collection of alpha-particle-generated carriers in silicon devices," *IEEE Electron Device Lett.,* vol. 2, no. 4, pp. 103-105, 1981.

[8] P. E. Dodd, F. W. Sexton, and P. S. Winokur, "Three-dimensional simulation of charge collection and multiple-bit upset in Si devices," *IEEE Trans. Nucl. Sci.,* vol. 41, no. 6, pp. 2005-2017, 1994.

[9] C. W. Gwyn, D. L. Scharfetter, and J. L. Wirth, "The analysis of radiation effects in semiconductor junction devices," *IEEE Trans. Nucl. Sci.,* vol. 14, no. 6, pp. 153-169, 1967.

[10] T. F. Wunsch and C. L. Axness, "Modeling the time-dependent transient radiation response of semiconductor junctions," *IEEE Trans. Nucl. Sci.,* vol. 39, no. 6, pp. 2158-2169, 1992.

[11] D. J. Roulston, N. D. Arora, and S. G. Chamberlain, "Modeling and measurement of minority-carrier lifetime versus doping in diffused layers of n+-p silicon diodes," *IEEE Trans. Electron Devices,* vol. 29, pp. 284-291, 1982.

[12] L. W. Massengill and S. E. Diehl-Nagle, "Transient radiation upset simulations of CMOS memory circuits," *IEEE Trans. Nucl. Sci.,* vol. 31, no. 6, pp. 1337-1343, 1984.

Distribution:

1 Wendland Beezhold
Idaho State University
Physics Department
Pocatello, ID 83209

1 MS 0188 D. L. Chavez, 1011
1 MS 0316 H. J. Hjalmarson, 9235
1 MS 0525 S. D. Wix, 1734
1 MS 0525 P. V. Plunkett, 1734
5 MS 1056 G. Vizkelethy, 1111
1 MS 1056 D. S. Walsh, 1111
1 MS 1056 D. L. Buller, 1111
1 MS 1056 B. Doyle, 1111
1 MS 1167 K. M. Horn, 15343
1 MS 1179 J. R. Lee, 15340
1 MS 1179 D. E. Beutler, 15341
1 MS 1081 C. E. Hembree, 1739
1 MS 1081 F. W. Sexton, 1762
5 MS 1083 P. E. Dodd, 1762-1

1 MS 9018 Central Technical Files, 8945-1
2 MS 0899 Technical Library, 9616
1 MS 0612 Review & Approval Desk, 9612
For DOE/OSTI
1 MS 0188 D. Chavez, LDRD Office, 1030